Delft University of Technology

The use of subsurface for thermal energy transport in district networks

Student: Kaixuan Jiang
Supervisors: Mark Bakker
Martin Bloemendal
Niels Hartog
Boris van Breukelen

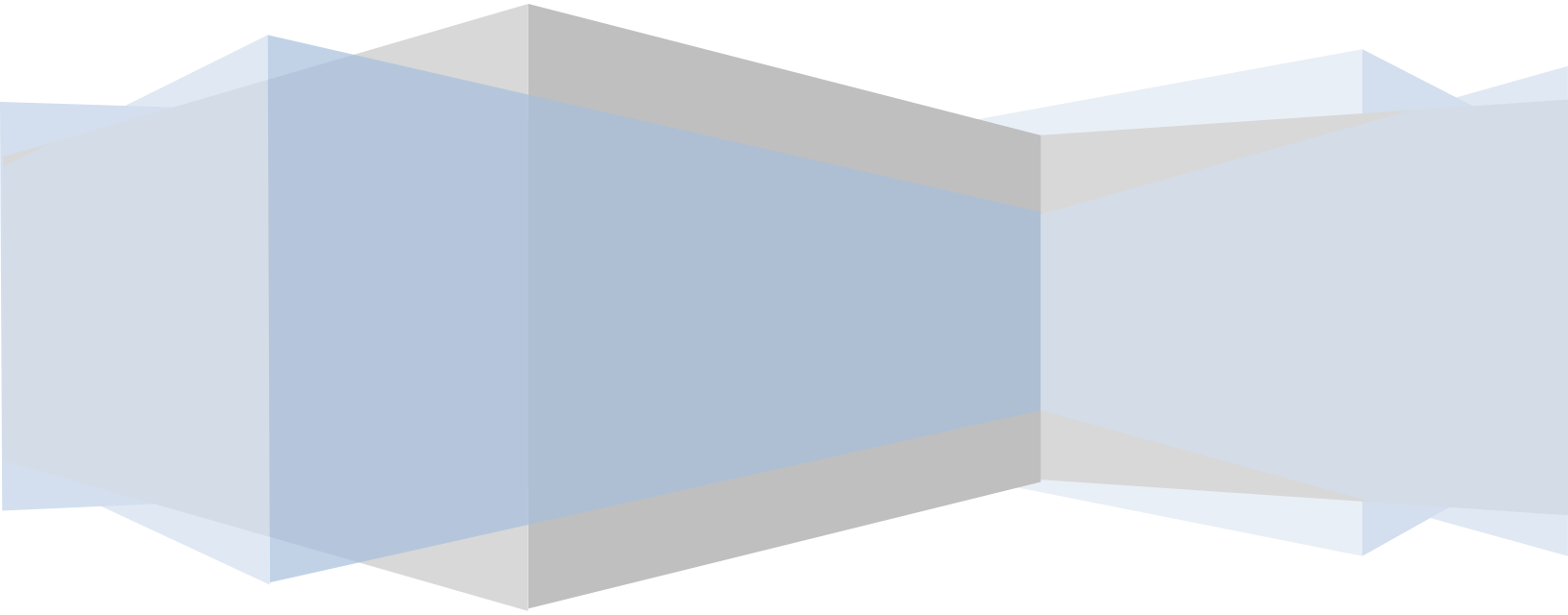

Content

Abstract

This study introduces a new concept of ATES system, which is called ATEST system, to fulfill the transport function while crossing the barriers in water transmission and pipe replacements. Firstly, analytical models were used to help understand the physical process and range the working conditions of the ATEST system. Then numerical models were used to prove the feasibility and the value of this new conceptual system. Acceptable system performance that can meet the heat demand was iterated in case simulation; and the economical advantages were identified by comparing it with traditional ATES systems. The ATEST system showed a greater practical value than the ATES system in: 1) solving the discrepancy between heat service and heat demand in space, and 2) crossing barriers where pipes cannot be buried. However, the system should be further modified in operation to acquire better performance and avoid practical problems.

1. Introduction

According to Plc (2016), there is now an increasing demand for energy because the world economy continues to grow. This has caused energy scarcity as well as many environmental problems like greenhouse gas (GHG) emissions. Novo et al. (2010) stated that, according to energy policies issued by some authoritative world organizations, many governments and companies are striving to develop renewable energy and reduce fossil energy use to cut GHG emissions.

Currently, according to Sanner et al. (2003) and Novo, Bayon et al. (2010), the subsurface is increasingly used for thermal energy storage, which is referred to as the underground thermal energy storage. Sommer et al. (2015) confirmed that this is a cost-effective technology that reduces energy use and the GHG emissions. Bloemendal et al. (2014) introduced that the aquifer thermal energy storage (ATES) system is a specific type of thermal energy storage, which stores energy in aquifers: cold water is extracted and warm water is injected after heat exchange in summer, while in winter, the process is reversed to supply sustainable heat to the buildings.

The ATES systems use subsurface for storage solely, to bridge the discrepancy between demand and availability of heat in time. Because aquifers are continuous layers, they may also be used to transport heat, which could be quite useful in district heating networks, where heat needs to be transported from one area to another, and buffering is needed for redundancy or temporal storage. In this research, a new ATES concept with transport function is introduced — the aquifer thermal energy storage & transport (ATEST) system. The ATEST system can be beneficial for district heating networks, especially when it needs to cross a canal or other infrastructure facilities, which would normally be expensive for a pipe network. Meanwhile, the aquifer storage keeps its buffering function so as to create redundancy between heat demand and production and/or limit dependence.

The main objective of this research is to identify the possibility of the ATEST being a viable technology for storing and transporting large quantities of thermal energy. This is done by:

1. Identifying the conditions under which ATEST should work,
2. Setting up assessments standards and modeling frameworks for evaluating its performance,
3. Running simulations to identify ATEST's performance under a series of different conditions,
4. Designing a case/pilot ATEST system, and then
5. Evaluating the practical feasibility and value of the ATEST system.

2. Research approach

To meet the research objective, analytical and numerical simulations were used to explore how ATEST systems can work and which parameters are of crucial importance for the feasibility.

1. To allow for simulation and comparison, it is necessary to collect the required data as well as identify research tools and methods, which are presented in chapter 3.
2. The results of analytical models are shown in chapter 4, from which the basic working process and narrowed working conditions were concluded.
3. The results of numerical models are shown in chapter 5, which were concluded from more practical conditions and more detailed sensitivity analysis.
4. Finally, in Chapter 6, a case simulation shows the feasibility of an ATEST system in a concrete setting.

The strategy of this research is schematically represented in Figure 1.

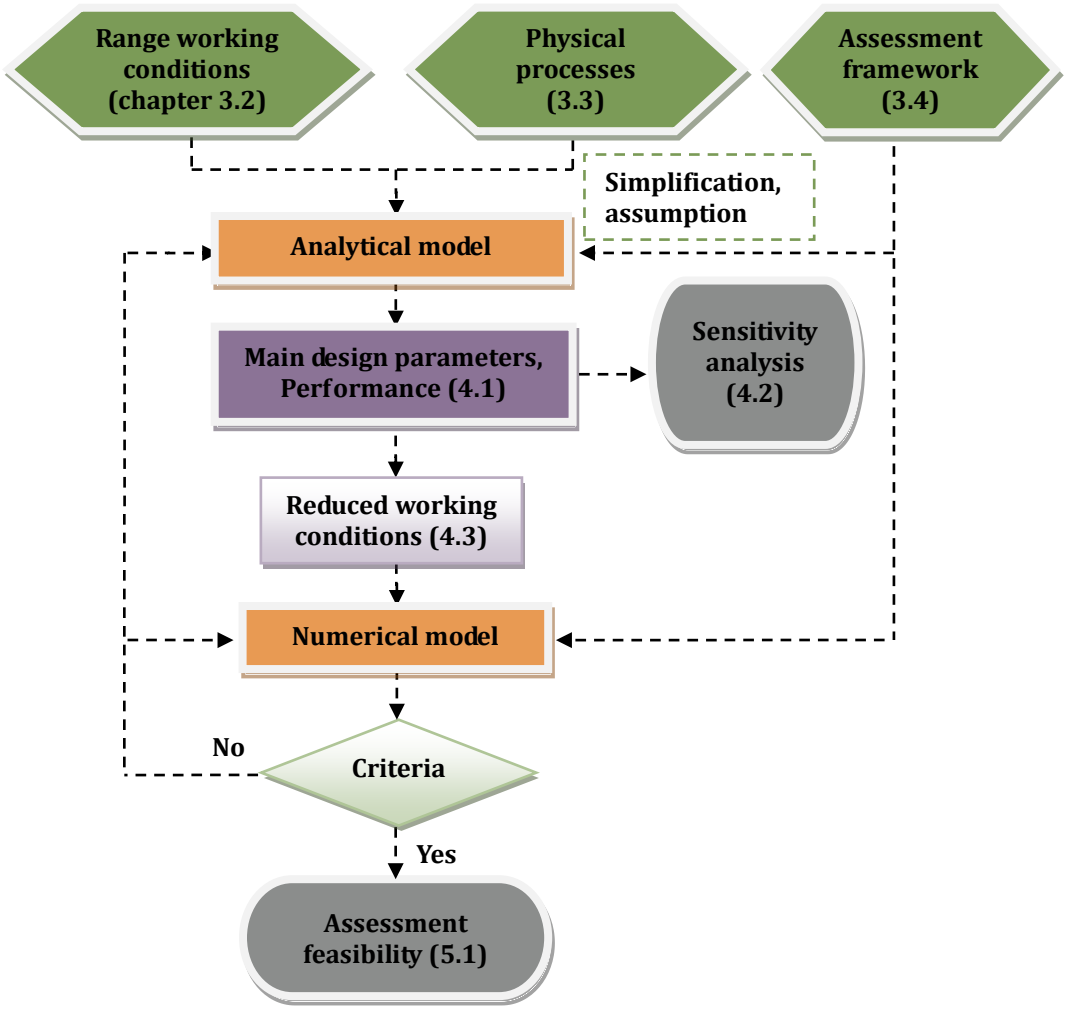

Figure 1. Research approach

2.1. Identification / collection of required data, tools and methods

Technology comparison

Firstly, it was necessary to carry out a technology comparison by listing and comparing the technology of the ATEST with the traditional ATES and HT-ATES systems, to identify the differences and advantages of the ATEST system. This was done in section 3.1.

Identifying governing processes of the ATEST system

The dominant physical processes were identified in section 3.2. And those that were relevant to the ATEST systems included:

- Flow in porous media & groundwater well technology
  Subsurface is regarded as a porous medium, and the flow inside it is significantly influenced by its properties (porosity, permeability, etc.) and the pumping in wells.

- Heat transport / Thermodynamics
  Heat transport is significantly correlated with hydraulic transport, but the principles are much more complex. Identifying heat transport is essential to measuring energy loss, efficiency and thermal travel time.

- Density and viscosity differences
  Considering the effect of temperature on water density and viscosity, changes in the two aspects under different temperature conditions were discussed as well to make the model more accurate.

Defining working conditions for the ATEST systems

The working conditions of the ATEST systems are similar to those of the ATES systems. Basic working conditions for the ATEST system were defined in section 3.3, followed by the analysis.

Based on literature, practical experiences and operating timetables of existing ATES, HT-ATES and district heating networks, parameter values were identified in the following aspects:

- Thermal energy production information (e.g. CHP)
- Thermal energy demand profiles
- Temperature level of storage
- Geographical conditions
- Geo-hydrological conditions

Scenarios were defined based on this inventory and then tested in the analytical and numerical simulations.

Assessment criteria

To allow for comparison of results, assessment criteria need to be defined. In section 3.4, three types of criteria were used to evaluate the performance of the ATEST systems, namely, thermal travel time, efficiency and water balance.

1) Thermal travel time
   In the ATEST system, it may take some time to transport the infiltrated warm water from one place to another. This criterion was used to assess the system's performance mathematically together with efficiency.

2) Efficiency
   Efficiency is an important criterion because it is beneficial to extract as much stored heat as possible. Efficiency can be described and calculated mathematically. However, in the analytical model, efficiency is transformed and represented by some other indexes because it is difficult to simulate energy transport.

3) Water balance
   Water balance should be considered as a criterion of performance, since water is injected and extracted in different places in the ATEST system. This issue was mathematically analyzed only in terms of the geo-hydrological aspect.

Analytical modeling framework

Analytical simulation is very powerful in gaining understanding of the processes and identifying dominating parameters. Governing equations were simplified in this research to allow for simulating of a wide range of working conditions within the limited time.

The structure of analytical model was described in section 3.5. In the simulation, analytical models were prior established based on the working conditions and constraints.

Numerical modeling framework

Numerical simulations were used to study the dynamic effects of groundwater and heat transport simultaneously to get more reliable and valuable results. In numerical models, the integrated transport processes were simulated. The Numerical modeling framework was described in section 3.6.

2.2. Simulation results and sensitivity analysis

Analytical simulation results

The analytical simulation results consisted of the critical processes, design conditions, key operation conditions and control parameters. This was done in Chapter 4.

The influences of different parameters were studied by stepwise changing under the working conditions, and then the sensitivity analysis provided insight in the interdependencies of different parameters.

Numerical simulation results

The results from numerical simulation were described in Chapter 5, which were more practical and accurate and could be directly used to evaluate system feasibility.

2.3. Case simulation

In Chapter 6, the ATEST system was studied in a case project with the district heating network of TU Delft. This was carried out to test whether a system in the case project would follow the identified behavior and thus validate the outcomes of the analytical and numerical simulations, and to identify practical aspects which had not been considered during the simulation study.

This study was conducted by computer simulation. Firstly, the geological properties in the target area were identified based on the geology database, and the heat production and demand were decided to determine the scale and layout of the ATEST system. Then the target place was simulated based on the geological survey, and the desirable system performance was iterated by the numerical modeling. Finally, the assessment criteria defined above were used to evaluate the feasibility of the ATEST system.

3. Data, research tools and methods

3.1. Technology of ATES and ATEST

3.1.1. ATES

Paksoy (2007) mentioned that the first reported subsurface thermal energy storage was in China in the 1960s. Following studies were conducted in Japan and France by Tsang (2012) and Bonte et al. (2013) respectively. Paksoy (2007) commented that, currently, the Netherlands and Sweden are dominant in the implementation of this method. According to Willemsen (2016), in the Netherlands, 8000 ATES systems are expected to have been installed until 2020, which will save 4% of the total energy consumption.

Nordell et al. (2015) introduced that, currently, the heating / cooling capacity from storage of the ATES systems is 500-2000KW, with the groundwater flow between 1000-5000m^3/d. Generally, according to Zeghici et al. (2015), the temperature of groundwater for cooling in summer is below 10°C, while that for heating is between 15°C and 25°C, with a pump working to heat or cool the water for different uses.

Compared with geothermal energy mining, ATES is a rather energy-saving system, because although it cannot generate extra energy, it stores the excess heat for future use. In the ATES systems, cold water is extracted for cooling during summer, and warm water is injected into the aquifer, while, in winter, warm water is extracted for heating and cold water is injected for the next summer. Figure 2 shows the general principle of the ATES system. Bloemendal and Olsthoorn et al. (2014) added that, to obtain an optimal use of subsurface space and high recovery efficiency, the wells should be set close to each other.

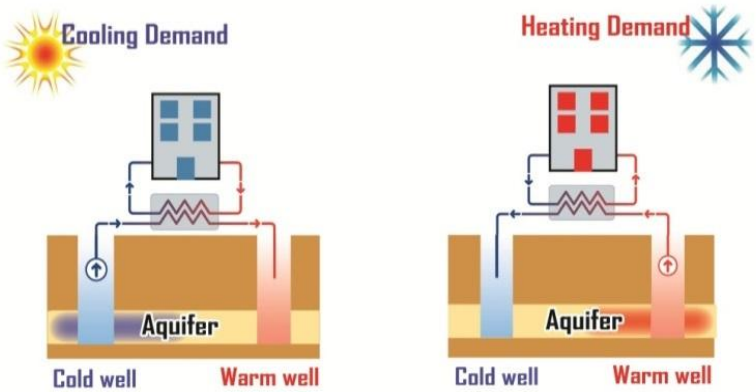

Figure 2. The principle of ATES

3.1.2. HT-ATES

According to Sanner et al. (2005), at present, the only active HT-ATES system in the world is in Berlin. Wesselink (2016) added that there had been two projects with storage temperatures over 80°C in the Netherlands, but both of them were closed due to practical problems. Drijver et al. (2012) explained that the HT-ATES system is not yet fully developed, but has received a lot of attention in recent years because of its potential to utilize the high exergy heat.

In the HT-ATES system, warm water is of a higher temperature (usually over 40°C), and the system is only used for warm water storage and recovery. According to Drijver and Aarssen et al. (2012), compared with the conventional ATES systems, the recovery efficiency of the HT-ATES system is lower, but the extracted warm water can be directly used without heat pumps.

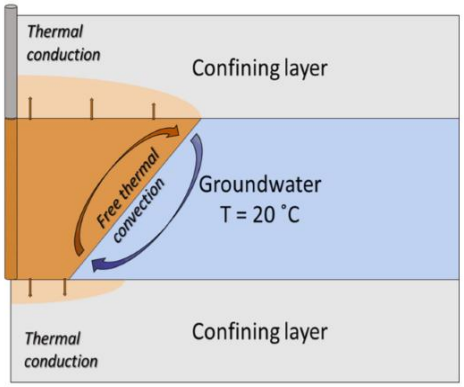

Figure 3. The density driven flow in the HT-ATES system (van Lopik et al. 2016)

One problem of the HT-ATES system is the serious heat loss from the density driven flow, because the warm water tends to flow upward (figure 3), and cannot be recovered efficiently in aquifer due to the fact that water in a higher temperature has a lower density. Van Lopik and Hartog et al. (2016) pointed out that this can be solved by using salt to set off the density change from temperature difference. Drijver (2011) added that another problem is the chemical changes (precipitation of mineral, corrosion, etc.) due to high temperature. But this can be avoided using some water treatment methods.

3.1.3. ATEST

In addition to heat storage, the ATEST system can transport warm water from one area to another via the aquifer, which involves very special physical processes of the groundwater. The ATEST system transports water of a high temperature (>70°C), and the warm water is promoted by groundwater flow inside the aquifer, which may be

generated artificially. The principle of the ATEST system is shown in Figure 4.

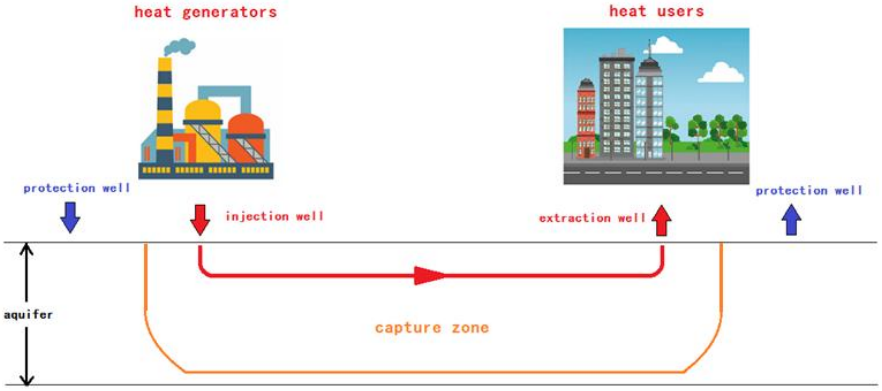

Figure 4. The principle of ATEST

Considering the heat loss during the transport process, the recovery efficiency of the ATEST system may be lower than that of the ATES system. However, the ATEST system can save a lot of investment costs, mainly from pipe-laying and installing projects, because water is transported in aquifer instead of pipes.

3.2. Governing processes

3.2.1. Flow of water and heat in porous media

Porosity

Porosity is the ratio between the volume of the space and the total volume defined as:

$$n = \frac{V_v}{V_t} \quad \dots \quad 1$$

where n is porosity [-], V_v is the void volume [m^3], and V_t is the total volume [m^3].

Porosity is an important property of the aquifer for subsurface flow and bulk specific heat capacity. In case of high porosity, the groundwater flow is retarded but the bulk specific heat capacity is larger. Generally, according to Fitts (2003), the porosity is 5-30% for sandstone, 30-50% for narrowly graded silt, sand and gravel, and 35-60% for clay.

Grain size, intrinsic permeability and hydraulic conductivity

In unconsolidated materials, the grain size is a significant property. According to Fitts (2003), the grain size is 0.05-2mm for sand material, and over 2mm for gravel material. The intrinsic permeability of the aquifer is proportional to the grain size. Therefore, when the material is coarse, there is lower resistance to the underground flow, and the

intrinsic permeability is high.

Hydraulic conductivity is generally used in calculation, which can be derived from grain size or intrinsic permeability. The equation below was proposed by Price et al. (1911) to show the relationship between grain size and hydraulic conductivity:

$$K = C(d_{10})^2 \quad \dots \quad 2$$

where K is the hydraulic conductivity [m/d], C is a constant number [$/m \cdot d$], and d_{10} is the grain size that is larger than 10% grains in the material.

In equation 2, the constant number 'C' is obtained through experiment and derivation, which is influenced by many factors and varies with different materials, so usually another equation proposed by Hubbert (1940) is used:

$$k = \frac{K\mu}{\rho_w g} \leftrightarrow K = \frac{\rho_w g k}{\mu} \quad \dots \quad 3$$

where k is the intrinsic permeability [m^2], μ is the dynamic viscosity [N•s/m^2], ρ_w is the density of water [kg/m^3], and g is the gravitational acceleration [m/s^2].

Darcy's law

Darcy's law describes the relationship among subsurface flow, hydraulic conductivity and hydraulic gradient. This law was adopted in this research to dominantly identify the geo-hydrology as:

$$Q = -KA\frac{dh}{ds} \quad \dots \quad 4$$

In this equation, Q is the discharge of subsurface flow [m^3/d], K is the hydraulic conductivity [m/d], A is the cross section for flow [m^2], and dh/ds is the hydraulic gradient [-].

Darcy's law can also be used in 3-D conditions as follows:

$$\begin{cases} q_x = -K_x\frac{\partial h}{\partial x} \\ q_y = -K_y\frac{\partial h}{\partial y} \\ q_z = -K_z\left(\frac{\partial h}{\partial z} + \frac{\rho_w - \rho_f}{\rho_f}\right) \end{cases} \quad \dots \quad 5$$

In equation 5, q is the specific discharge [m/d], $\partial h/\partial i$ is the hydraulic gradient [-], ρ_w is the water density at the bottom of subject cubic [kg/m^3], ρ_f is the water density at the top [kg/m^3].

Darcy's law is valid for a continuum. In the equations, the hydraulic conductivity and hydraulic gradient are constant. If the subject is not large enough, irregularities (hydraulic conductivity, hydraulic gradient) will occur inside and prevent the Darcy's law from working. Another assumption of Darcy's law is laminar flow proposed by Fitts (2003). Parlange (1973) added that the experiments from Bear showed Darcy's law is not valid unless the Reynolds number of flow is below a certain value between 1 to 10.

3.2.2. Heat transport

Conduction and advection are two dominant patterns of thermodynamics. During the transport process, thermal energy firstly heats the existing phase, and then continuously diffuses and disperses at the system boundary.

Conduction

Thermal conduction is the transfer of heat (internal energy) by microscopic collisions of particles and movement of electrons within a body[1]. When two bodies are relatively static and in touch with each other, the conduction is the main thermodynamic process in heat exchange.

Thermal conduction is described by Fourier's law as:

$$q_c = -\lambda \frac{dT}{ds} \quad \ldots \quad 6$$

where q_c is the energy conducted per unit area [W/m^2], λ is the thermal conductivity [W/m°C], and dT/ds is the temperature gradient [°C/m]. Generally, the thermal conductivity is isotropic in one body, which is assumed as $\lambda_x=\lambda_y=\lambda_z$.

According to Fitts (2003), in subsurface, the media have multiple phases — a solid mineral matrix with liquid pore fluids. The bulk thermal conductivity should be measured by using the empirical equation below proposed by Ingebritsen et al. (1998):

$$\lambda = (\lambda_m)^{1-n}(\lambda_f)^n \quad \ldots \quad 7$$

where λ is the bulk thermal conductivity [W/m°C], λ_m is the thermal conductivity of the matrix (solid phase) [W/m°C], λ_f is the thermal conductivity of water (liquid phase) [W/m°C], and n is the porosity.

Advection

Energy advection in the aquifer is the process that energy moves in the medium of energy-stored water [2], which is described by the equation below proposed by Fitts (2003):

$$q_a = q\rho H \quad \ldots \quad 8$$

In this equation, q_a is the advective energy flux [W/m^2], q is the specific discharge of water [m^2/s], ρ is the water density [kg/m^3], and H is the enthalpy of water [J/kg].

Integrated thermal energy transport

For energy transport, advection, dispersion and diffusion (conduction) are the three dominant processes. Thorne et al. (2006) proposed a temperature transport solution as follows:

$$\left(1 + \frac{1-n}{n}\frac{\rho_s}{\rho}\frac{c_s}{c_f}\right)\frac{\partial(nT)}{\partial t} = \nabla\left[n\left(\frac{\lambda}{n\rho c_f} + a\frac{q}{n}\right)\nabla T\right] - \nabla(qT) - H \quad \ldots \quad 9$$

[1] https://en.wikipedia.org/wiki/Thermal_conduction
[2] https://en.wikipedia.org/wiki/Heat_transfer#Advection

where n is the porosity [-], ρ_s is the density of solid [kg/m^3], ρ is the density of fluid [kg/m^3], c_s is the heat capacity of solid [J/kg/K], c_f is the heat capacity of fluid [J/kg/K], α is the dispersion coefficient [m], q is the specific discharge [m^2/s], and H is the enthalpy of source. In this equation, advection, conduction and dispersion are all considered, and the energy change in these three processes equals the change of the system's internal enthalpy.

Enthalpy is the sum of the total kinetic (thermal) energy, the total potential energy and the total work to surroundings, described as follows:

$$H = U_k + U_p + \frac{P}{\rho}$$

If the system is chemically inert, the total enthalpy can be regarded as equivalent to the kinetic (thermal) energy, as in $H=U_k$.

Ideal thermal transport

In the ATEST system, thermal energy is transported by advection, during which loss of energy into the surroundings occurs through dispersion and conduction. According to Doughty et al. (1982), in principle, the temperature profile is mainly shaped by advection, and the influence is shown in the figure below:

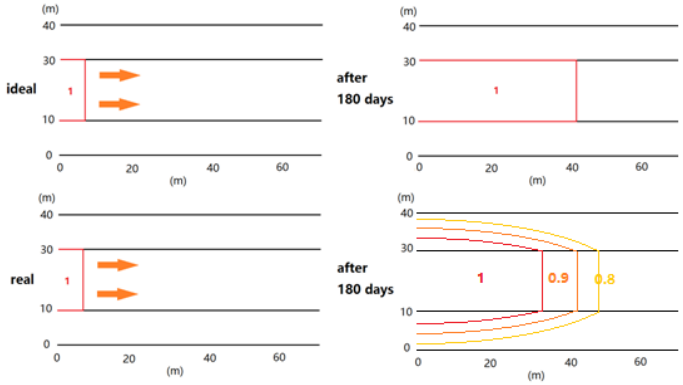

Figure 5. Thermal transport in ideal and real conditions

In the analytical simulation, it was acceptable to analyze thermal transport only with advection. With this simplification, thermal energy was always stored in the injection water, and the thermal transport was lagged behind the water transport, because the thermal energy in the front was used to heat the aquifer's original phase. According to Bloemendal et al. (2016), the thermal radius can be calculated from the hydraulic radius by equation 14. At the thermal boundary, it was assumed that the temperature suddenly rose because the background temperature was injected into the water temperature.

$$r_{th} = \sqrt{\frac{nc_w}{c_{aq}}} r_h \quad \ldots \quad 10$$

In this equation, r_{th} is the thermal radius [m], r_h is the hydraulic radius [m], n is the porosity [-], c_w is the heat capacity of water [J/kg/K], and c_{aq} is the heat capacity of the aquifer [J/kg/K],which is obtained as follows:

$$c_{aq} = nc_w + (1-n)c_s$$

where c_s is the heat capacity of solid phase.

3.2.3. Viscosity and density difference

In this research, viscosity and density changes in the water phase were considered. Water density was affected by temperature, pressure and salt concentration. However, according to Streeter et al. (1979), the compressibility of water is very low, at the 10^{-10} m^2/N level . Thus, water is generally considered incompressible. Furthermore, the water used in this research was assumed to be fresh water, so the density change due to salt concentration was neglected.

Viscosity change with temperature

In this research, because intrinsic permeability is an internal property of the aquifer, it was assumed as constant and continuous. According to equation 3, when the intrinsic permeability is constant, the hydraulic conductivity will depend on the liquid viscosity, and further affected by the temperature.

In experiments, the water viscosity changed dramatically along with the temperature, and, thus, it dominates the change of the hydraulic conductivity. Generally, when the temperature is between 20°C and 90°C, the water viscosity will decrease by about two thirds (from 1.002×10^{-3} to 0.315×10^{-3} Pa•s) and the hydraulic conductivity will increase about three times. The viscosity change can be described by the equation below proposed by Voss (1984):

$$\mu = 2.394 \times 10^{-5} \left(10^{\frac{248.4}{T+133.2}}\right) \quad \ldots \quad 11$$

where the unit of 'T' is °C.

Density change with temperature

Water density is highest at 4°C, and, when it is above 4°C, it is negatively correlated with temperature. In this research, a simple linear function proposed by Langevin et al. (2008) was used to simulate the water density with respect to temperature as follows:

$$\rho = 1000 - 0.392(T - 14) \quad \ldots \quad 12$$

3.2.4. Technology of wells

The wells in the ATEST system were used for water injection and extraction, as well as generation of the artificial groundwater flow. In this research, multiple wells were established and studied under both steady and transient conditions.

General equation in steady condition

In Figure 6, the groundwater flow is considered as constant along depth, so the 3-D real-life case could be simplified to a 2-D model. In the 2-D model, the layers at the aquifer's top and bottom were considered impermeable under the ideal condition.

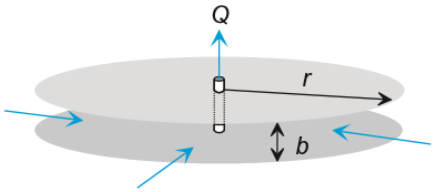

Figure 6. Radial flow to a well

The general equation for the water head around a well is:

$$h = \frac{Q}{2\pi T} \ln \frac{r}{r_0} + h_0 \quad \ldots \quad 13$$

where Q is the discharge/recharge of the well [m^3/d], r is the distance from well [m]. In case of $r=r_0$, the water head h equals h_0. And T is the aquifer transmissivity [m^2/d] as in T=Kb, where K is the hydraulic conductivity [m/d], and b is the depth of the aquifer [m].

Superposition

Superposition principle is used when there are multiple effects on groundwater, such as the existence of more than one well, or wells with ambient underground flow. The general Laplace equation is as follows:

$$h = \sum \frac{Q_i}{2\pi T} \ln r_i + Ax + By + C \quad \ldots \quad 14$$

where A, B and C are constant numbers, and 'x' and 'y' show the location of wells in the coordinates.

Two special layouts of wells were significantly useful in this research: one is two equal-discharge wells and the other is two inverse equal-discharge wells. In the ATEST system, these two layouts were used to generate and control the underground flow in combination. Figure 7 shows the headlines and streamlines for these two layouts.

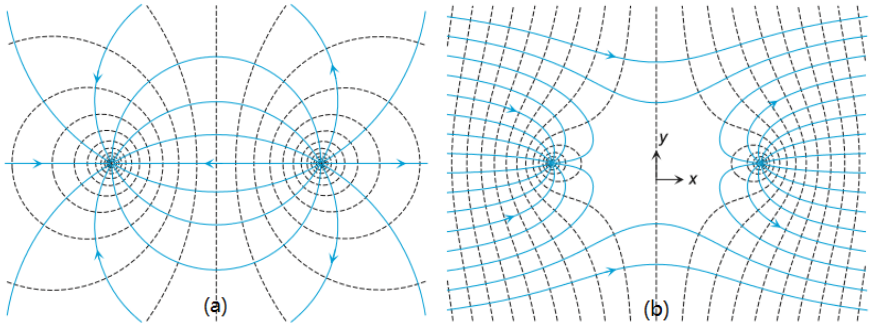

Figure 7: (a). Two same discharge inverse wells; (b). Two same discharge wells

Water head in transient condition

In the 2-D model, this solution was commonly used for the transient flow around a well, as was proposed by Theis (1935). The general transient solution is as follows:

$$h = h_0 - \frac{Q}{4\pi T} E_1(u) \quad \ldots \quad 15$$

where h_0 is the initial water head [m] at the subject point, Q is the discharge of the well [m^3/d], T is the aquifer transmissivity [m^2/d], $E_1(u)$ is the exponential integral function of u, and u is a dimensionless parameter:

$$u = \frac{r^2 S}{4T(t-t_0)}$$

When u is very small, an approximation can be used to calculate $E_1(u)$ as follows:

$$E_1(u) \approx -\gamma - \ln u$$

where γ (equals 0.5772) is the Euler's constant number.

In the transient solution, superposition for time and distance can be used as follows:

$$h = h_0 - \sum \frac{Q_i}{4\pi T} E_1(u_i) \quad \ldots \quad 16$$

where

$$u_i = \frac{r_i^2 S}{4T(t-t_i)}$$

3.3. Required working conditions of the ATEST systems

3.3.1. The scale of heat

Availability of heat

The ATEST systems are supposed to connect relatively large heat generators to multiple smaller heat consumers. In practice, according to Rathakrishnan (2005) and Toth et al. (2016), heat is often provided in a relatively constant rate jointly by heat and power plants, industries or geothermal mining wells, which were chosen as heat generators in this research. Generally, the heat is transported by water below 100°C, and mainly used for heating residential or green-house areas.

- Heat from power plants

  Power plants provide heating using gas or coal fired boilers. In current practice, according to Nishigaki (2005), units of 30-150 MW electrical capacity are commonly used. And CAN GÜLEN (2010) introduced that, after the process of power production, another 30-150MW worth of thermal energy is stored in water as waste heat. The waste heat is still at a high temperature (>90°C), which is consistent with the study of Brokx (2016) showing that the ATES systems, along with CHP plants, have injection water at over 83°C. Generally, according to India (2015), the annual average load factor in a thermal power plant is 0.6-0.7. As a result, with an output power of 30-150MW, 1.5 to 9×10^5MWh thermal energy is

generated each year. When the 90°C water is used as the medium and the reference temperature is 20°C, 5,000-30,000m^3 water is needed every day.

- Heat from geothermal mining
  According to Cloetingh et al. (2010), the Netherlands is located at a place with relatively low lithosphere thickness (about 100km) and very low integrated lithosphere strength, which is ideal for geothermal mining. Bonté et al. (2012) pointed out that, in the Netherlands, the temperature is roughly over 70°C at 2,000m depth underground, which is suitable for thermal energy mining. According to DiPippo (2016), due to the limitation of thermal conduction in geothermal reservoir, the energy production volume is between 5-6MW, or 4.4 to 5.2×10^4MWh annually. When the water at 90°C is used to transport the heat in the 20°C background, the discharge should be 1,000-2,000m^3/d.

It can be concluded that the injection water of an ATEST system is expected to be between 70°C and 90°C to be valuable for further distribution and usage, that the system can transport and supply thermal energy on a 10^4-10^5 MWh level, and that well discharges are determined at 5,000-30,000m^3/d for power plants and 1,000-2,000m^3/d for geothermal mining.

Demand for heat

According to Niessink et al. (2015), in the Netherlands, 13 heat distribution networks are defined on a large scale, and each of them connects 5,000 to 50,000 dwellings. Previous research has identified the individual heat demand to be about 23GJ/dwelling/year (6400kWh/year) for new buildings and 30GJ/dwelling/year (8300kWh/year) for old ones[3].

Therefore, annually, one residential area with 5-50 thousand families needs energy of about 3.2×10^4—4.2×10^5 MWh for heating. However, according to Zangheri et al. (2014) the heat demand is not constant around the year, but changes significantly in different seasons and climates. Specifically, heat demand concentrates in winter, and approximates to zero in summer. In practice, this change should be considered.

Niessink and Rösler (2015) indicated that the heat demand of dwellings is relatively flexible, because several types of heat sources can be used. Therefore, if the heat availability does not meet the demand, the figure of the heat generator should be referenced. .

[3] http://www.nle.nl/

3.3.2. Geological and geo-hydrological conditions

Geological condition

The study from Nordell and Snijders et al. (2015) showed that the ATES systems can be properly installed in the aquifers with high permeability, in which the range of particle size is 0.2-2mm, according to Sommer and Valstar et al. (2015). If the material size is too small and the aquifer permeability is too low, it will be hard to drive the subsurface flow, requiring a large hydraulic head difference. On the other hand, according to van Lopik et al. (2015) and Van Lopik, Hartog et al. (2016), if the soil is too coarse and the permeability is too high, large energy loss from groundwater movement cannot be avoided. In the Netherlands, generally, the aquifer consists of sand layers, of which the intrinsic permeability is in on a 10^{-11}-$10^{-10}m^2$ level[4]. When the temperature is 20°C, it matches $10^1 – 10^2$m/d of the hydraulic conductivity.

According to Paksoy et al. (2009) and Nordell and Snijders et al. (2015), ATES should be installed at a relatively shallow place in the aquifer, the depth of which is typically around 50m and mainly within 5-150m underground. The aquifer cannot be too shallow because of the injection pressure, and should also not be too deep in case it should increase the installation costs. To reach a large storage capacity, the aquifer should not be too thin, but there is no upper limitation. If the aquifer is too thick, only part of it will be used by the partially penetrating wells.

Porosity is an important soil property. From the equation Q = vA, where 'Q' is the discharge [L^3/T], 'v' is the velocity [L/T], and 'A' is the cross-section area [L^2], it can be learned that, with a constant discharge, a higher velocity will be reached if the cross-section area decreases. When the total cross-section (void area and solid phase) is constant, the porosity has the first-order influence on the real cross-section, as in $A_{real} = nA_{tot}$, where n is porosity [-]. According to Pluymaekers et al. (2012), the aquifer porosity in the Netherlands ranges from 0.2 to 0.4.

To assess the feasibility of the ATEST system, the aquifer of 10-200m thick was studied, together with a porosity ranging between 0.2-0.4 and a hydraulic conductivity of 10-100 m/d.

Geo-hydrological condition

In the ATES system, to achieve high recovery efficiency, the ambient underground flow should be minimized. In contrast, in the ATEST system, to achieve the transport function, a steady underground flow may be expected. The direction of this underground flow should follow the transport direction; otherwise it will have adverse effects.

To properly generate and control underground flow, the ATEST system should be built

[4] https://www.dinoloket.nl/en/subsurface-data

with confined aquifer. The operating difficulty usually increases with the extension of transport distance. In this research, the transport distance between 200-2000m was studied. To confine the hot water in a limited area, ambient underground flow was needed, whether existing naturally or artificially generated by additional wells, and hydraulic gradient was studied in the range 10^{-4}-10^{-3}.

Summary

In summary, the aquifer permeability between 10^{-11}-$10^{-10}m^2$, along with the aquifer thickness of the ATEST system within 10-200m should be studied. The target aquifer should be between 20m-200m underground to avoid groundwater seepage and lower the system costs. Besides, the transport distance in 200-2000m should be studied. To drive and shape the underground flow, hydraulic gradient would be determined to be between 10^{-4}-10^{-3}.

3.3.3. Conclusions of working conditions

There are some similarities in principles and structures between the ATEST system and the ATES system, therefore, the working conditions of the latter can be referenced by the former. In the energy aspect, the heat availability and demand of the ATEST system can be modeled after the large HT-ATES system, because it should be determined in the same way.

However, in geological and geo-hydrological aspects, the ATEST system is different, requiring aquifers with higher permeability and lower porosity, as well as the underground flow.

Working conditions for the ATEST system are summarized in Table 1.

Table 1. Working conditions for the ATEST system

Energy production/demand	5×10^{4}--5×10^{5}MWh/year
Injection temperature	70-90°C
Well discharge	4000-10000m^3/d
Aquifer depth	20 – 200 m
Aquifer thickness	10 – 200 m
Aquifer permeability	1×10^{-11}--2×10^{-10} m^2
Transport distance	200 – 2000 m
Hydraulic gradient	5×10^{-4}—1.5×10^{-3}

3.4. Assessment framework

3.4.1. Thermal travel time

Thermal travel time includes the shortest thermal travel time (t_s) and the longest thermal travel time (t_l), which, combined together, can determine the practical applicability of the system in different working conditions. The shortest travel time shows the time it takes for the heat to reach the extraction well, while the longest thermal travel time shows the time it takes for the extraction well to obtain hot water in all directions, before the system can start the required operation.

3.4.2. Efficiency

The feasibility of the ATEST system is described by the system efficiency.

In the analytical model, simulation was run only in the geo-hydrology aspect, where the system efficiency could not be calculated directly. Therefore, the index “system surface area / injection well discharge” (A_{tot}/Q) was used to describe the system efficiency. At the boundary, the ATEST system continuously lost energy by dispersion and conduction, so the total system surface area could be used to evaluate the rate of heat loss. The injection well discharge represented the rate of energy injection. Therefore, the system surface area / injection well discharge (A_{tot}/Q) could represent the total heat loss / total heat injection, where a lower A_{tot}/Q ratio indicated a better system.

In the numerical model, since energy transport was simulated, the temperature profile with time and location could be drawn, which could be directly used to calculate the efficiency. However, in the analytical model, it was predicted that the system surface area / injection well discharge (A_{tot}/Q) was able to represent the system efficiency, so A_{tot}/Q should also be calculated in the numerical model to prove its significance.

3.4.3. Water balance

A system that does not achieve water balance will face many problems in practice. Therefore, although water balance is not a main factor that influences system performance, it is quite significant practically. And solutions should be given in the case simulation.

3.5. Analytical simulation framework

Basic model

Analytical models were used to study the influences of different parameters on the ATEST system's performance and to get insight in its internal principles and working conditions. A 2-D single-layer model without heat transport was used. Six parameters were tested, namely, hydraulic conductivity (K), aquifer thickness (H), porosity (n), hydraulic gradient (dh/ds), discharge of injection and extraction well (Q), and the distance between two wells (d). The multi-aquifer analytic element model Tim^{ml} developed by Bakker (2015) was used.

The model consisted of two wells (one injection well, and one extraction well) and worked under the ambient underground flow. The structure of this model is shown in Figure 8.

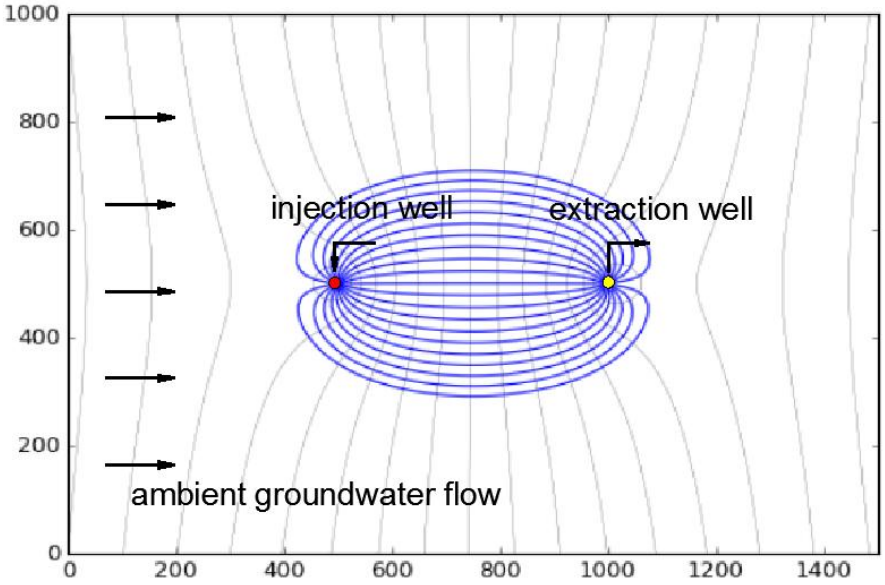

Figure 8. Profile of the basic analytical model

Stream line analysis was used for groundwater and heat transport. From equation 10, it is learned that the thermal radius is constantly proportional to the hydraulic radius. Thus, the thermal travel time can be derived reversely if the hydraulic travel time is known.

To obtain the hydraulic travel time, the points around the injection well were traced. One water particle on the right side and close to the injection well was traced, and the minimum hydraulic travel time it took to reach the extraction well was obtained. Then a water particle on the left side and close to the injection well was also traced, and the maximum hydraulic travel time it spent in reaching the extraction well was recorded. In simplification, a point at the upper (or lower) left position of injection well was traced, and, thus, the "longest travel time" was not the exact longest one.

To calculate A_{tot}/Q, the perimeter and area of a capture zone should be known. In this model, the shape of the capture zone was approximated as an ellipse, then the perimeter and area could be calculated as follows, after long axis and short axis were known:

$$P = \pi B + 2(A - B) \quad \ldots \quad 17$$

$$a = \frac{\pi AB}{4} \quad \ldots \quad 18$$

where A is the length of long axis, B is the length of short axis, P is ellipse's perimeter and a is the area. Subsequently, the system surface area equaled "2a + PH", where H is the aquifer thickness.

The discharge of the two wells were the same, so the long axis was the distance between two stagnation points, and the short axis was the width of the capture zone at x = 0. In this simple model, the long axis was calculated analytically. For the short axis, the vertical line at x = 0 was followed to firstly calculate the velocities of groundwater flow in x direction, and then separate this vertical line with 1m step by step. In each step, the discharge in x direction was calculated via $Q_x = v_x WH$, where W is the step width (1m) and H is the aquifer thickness. Finally, Q_x from (0, 0) was integrated to both sides in y direction, until $\sum Q_x$ equaled the well discharge, and the accumulated length was the width of the capture zone (short axis).

Within the working conditions defined above, the influences of the six parameters were studied by controlling variables. Specifically, five parameters were set as constant and the other one was adjusted, to record and evaluate the changes of criteria (t_s, t_l, A_{tot}/Q). Furthermore, multiple influences of the several parameters were studied by setting at most four parameters as constant and changing at least two parameters simultaneously.

With protection wells

In practice, positive ambient underground flow is not common, implying that protection wells should be used to drive the warm water artificially. To study a system with artificial underground flow, it is important to identify the methods to transform and assess the influence from protection wells.

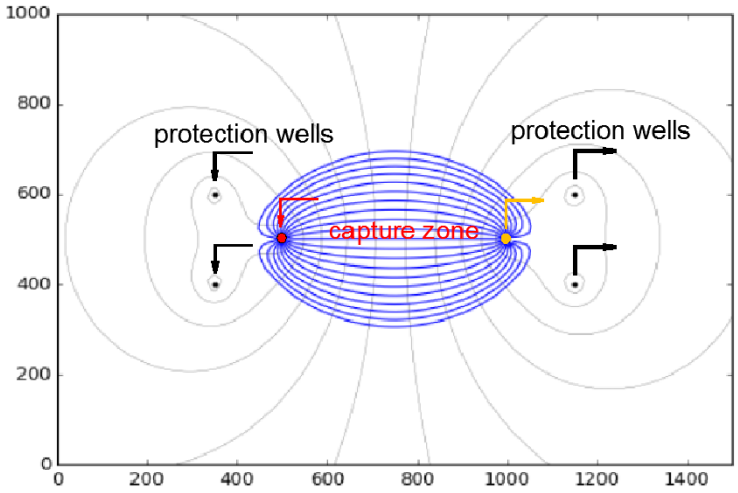

Figure 9. Analytical model with four protection wells

In Figure 9, the two main wells are bounded by four protection wells. The additional wells are called “protection wells” because they generate underground flow and separate the injection well’s hot water from the cold background to avoid thermal energy loss.

In simulations, when there were more than 2 wells, the stagnation points would be difficult to locate, making it impossible to calculate A_{tot}/Q. To solve this problem, the artificial hydraulic gradient from the protection wells was assumed to be constant, then the model could be regarded under the ambient underground flow (with constant dh/ds). And the methods to calculate t_s, t_l and A_{tot}/Q were the same.

3.6. Numerical simulation framework

After the analytical simulation, the study became more specific, where the physical processes were understood and a rough range of working conditions could be estimated. However, the energy transport was under the ideal condition in analytical models, neglecting some essential temperature-relative changes in aquifer properties. To make the ATEST system more reliable, dynamic processes in the geo-hydrology and energy aspects should be simultaneously studied in 3-D numerical models, from which the interaction between hydrology and energy could be discovered to yield more accurate results.

In the numerical simulation, a MODFLOW model for geo-hydrology modeling and a MT3DMS model for energy transport modeling proposed by Harbaugh (2005) and Verkaik et al. (2011) were established together. To consider the change of water density

along temperature, these two models were run alternately under the SEAWAT project developed by Langevina and Thorne Jr et al. (2008).

The profile of the MODFLOW model is shown in Figure 10. Horizontally, the target area is distributed by 100m×100m squares in the open space and 5m×5m squares at the wells, while, in between, the cell size increases from 5m to 100m by logarithm. Vertically, the model is distributed in 22 layers, with the top (constant water head and temperature) and bottom layers (impermeable) representing the system boundaries (H=1m). The 2nd-6th layers (H=10m) and 12th-16th layers (H=4m) represent confining layers, in which the horizontal hydraulic conductivity is 0.005m/d and the vertical hydraulic conductivity is 0.0005m/d based on practice (Hart et al. 2006, Timms et al. 2014). The 7th-11th layers are the main layers used for heat transport, forming one aquifer layer with the same properties. The 17th-21th layers form another aquifer layer, which is used for cold water transport to achieve water balance. During working time, hot water is injected through the injection well and cold water is injected through the injected protection wells (NO.1 and NO.2). Meanwhile, groundwater is extracted by the extraction well and extracted protection wells (NO.3 and NO.4). At the six places with wells, the supplementary wells in the deeper aquifer always have inverse equal discharge.

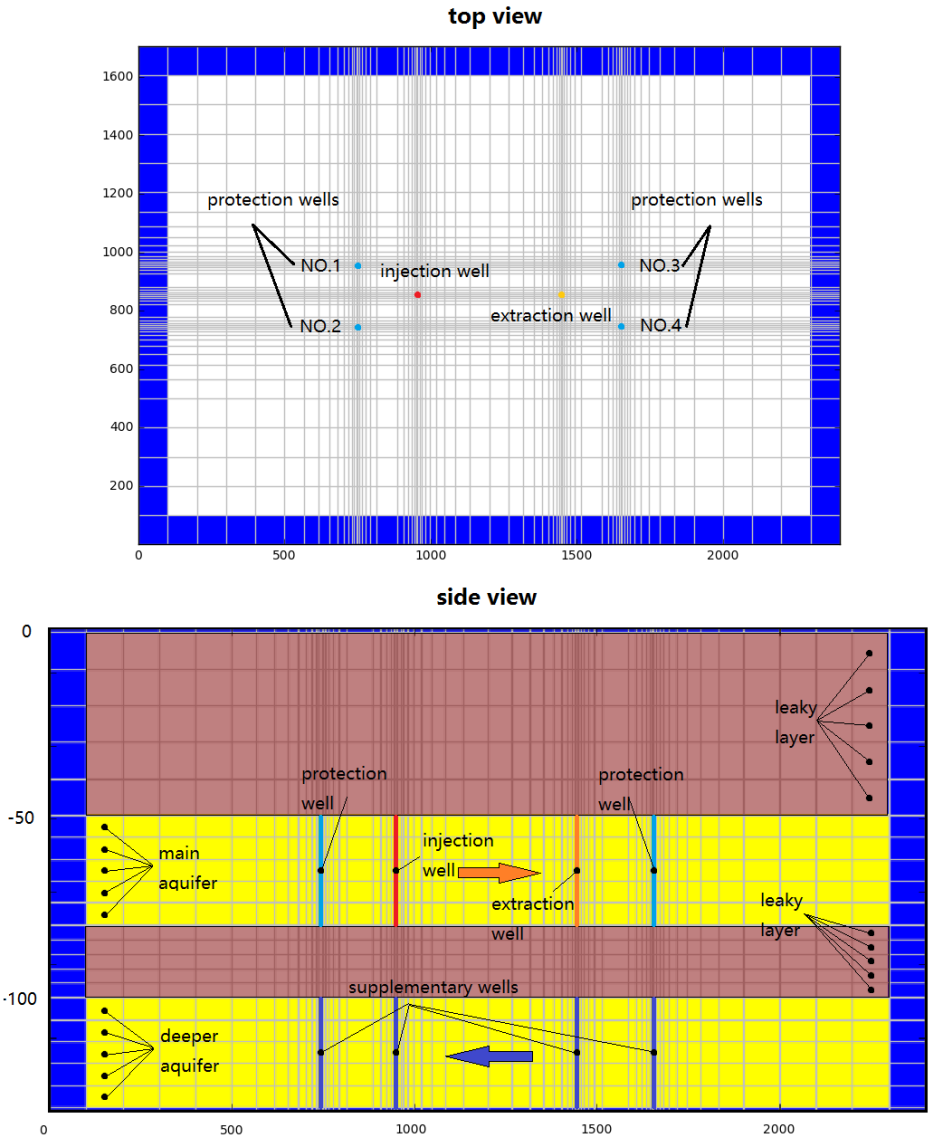

Figure 10. Distribution of the MODFLOW model

Energy transport processes were executed by MT3DMS. Fresh water was 20°C in the background and hot water was constantly 90°C in the injection well, and the forward-tracking method was used during heat transport. Dispersion coefficient was low in the medium with low Peclet number (Lee et al. 2007). Thus, in the MT3DMS model this coefficient was set at 0.5m horizontally and 0.05m Vertically. And the heat diffusion coefficient is set at 1.43e-7 m^2/s (Blumm et al. 2003).

The area far from the ATEST system maintained background water head and temperature, where heat was quickly exchanged into atmosphere at ground surface. Therefore, in the simulation, the model's top and surrounds were set in constant hydraulic head (i.e. 0m) and constant temperature (20°C). To avoid the influence from deeper underground, the model bottom was set as impermeable and isolated.

The MODFLOW and MT3DMS models alternatively ran under the SEAWAT project with 1/8 year in each step. Based on equation 12, water density decreases by -0.392kg/m^3 with one rising degree. According to equation 3 and equation 11, in each running cycle, the hydraulic conductivity is updated from new temperature data (the results from the last running cycle).

Thermal travel time

In numerical models, water temperature with time at the extraction well was plotted. Thermal travel times (t_s and t_l) could be calculated based on this temperature graph.

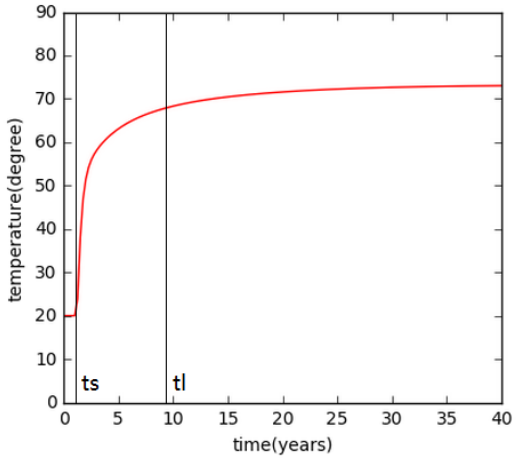

Figure 11. Temperature with time at the extraction well

Before heat reached the extraction well, the temperature of the well equaled background temperature (20°C). And a steady condition was achieved after a long time, when the temperature reached a specific value (about 73°C in Figure 11). The operating conditions of the ATEST system can be described by the transient temperature difference over the final temperature difference, as follows:

$$N = \frac{T_\tau - T_b}{T_f - T_b} \quad \dots \quad 19$$

In this equation, T_τ is the transient temperature at the extraction well, T_f is the final temperature at the extraction well, and T_b is the background temperature. When N=0, the water temperature is 20°C, implying that no heat reaches the extraction well, while the ATEST system reaches its optimal efficiency when N=1. In the simulation, the shortest and longest thermal travel time were defined when N=0.1, and N=0.9 respectively.

System total surface/injection well discharge

System efficiency could be calculated directly in the numerical models, so system total surface / injection well discharge (A_{tot} / Q) should be proved reasonable (correlated with efficiency) firstly, and then be used to link analytical results.

System surface area can be calculated by integrating the area of qualified cell, as follows:

$$M = \frac{T_{cf} - T_b}{T_f - T_b} \quad \dots \quad 20$$

In this equation, T_{cf} is the final temperature in each cell. A cell's area will be considered inside the warm zone when M>0.8.

Efficiency

The final system efficiency can be directly calculated by the equation below:

$$\eta = \frac{T_f - T_b}{T_i - T_b} \quad \dots \quad 21$$

In this equation, T_i is the temperature at the injection well. In practice, the injection well has worked for a long time, and much heat has been injected and stored in aquifer before the warm water can be extracted. Therefore, accumulated system efficiency may be more significant to describe the integral system performance. This criterion can be calculated by:

$$\eta_a = \frac{\int_0^t (T_\tau - T_b)dt}{\int_0^t (T_i - T_b)dt} \quad \dots \quad 22$$

In the simulation, the system was executed for 12 years.

4. Results from analytical simulations

4.1. System performance from single parameter

A basic tim[ml] model was established as a reference case with hydraulic conductivity (K)=50m/d, aquifer thickness (H)=100m, porosity (n)=0.3, hydraulic gradient (dh/ds)=0.001, discharge of wells (Q)=4000m^3/d, and transport distance (d)=500m. In the analytical model, six parameters (K, H, n, dh/ds, d, Q) were tested separately, and the influences of each parameter are shown in Figure 12.

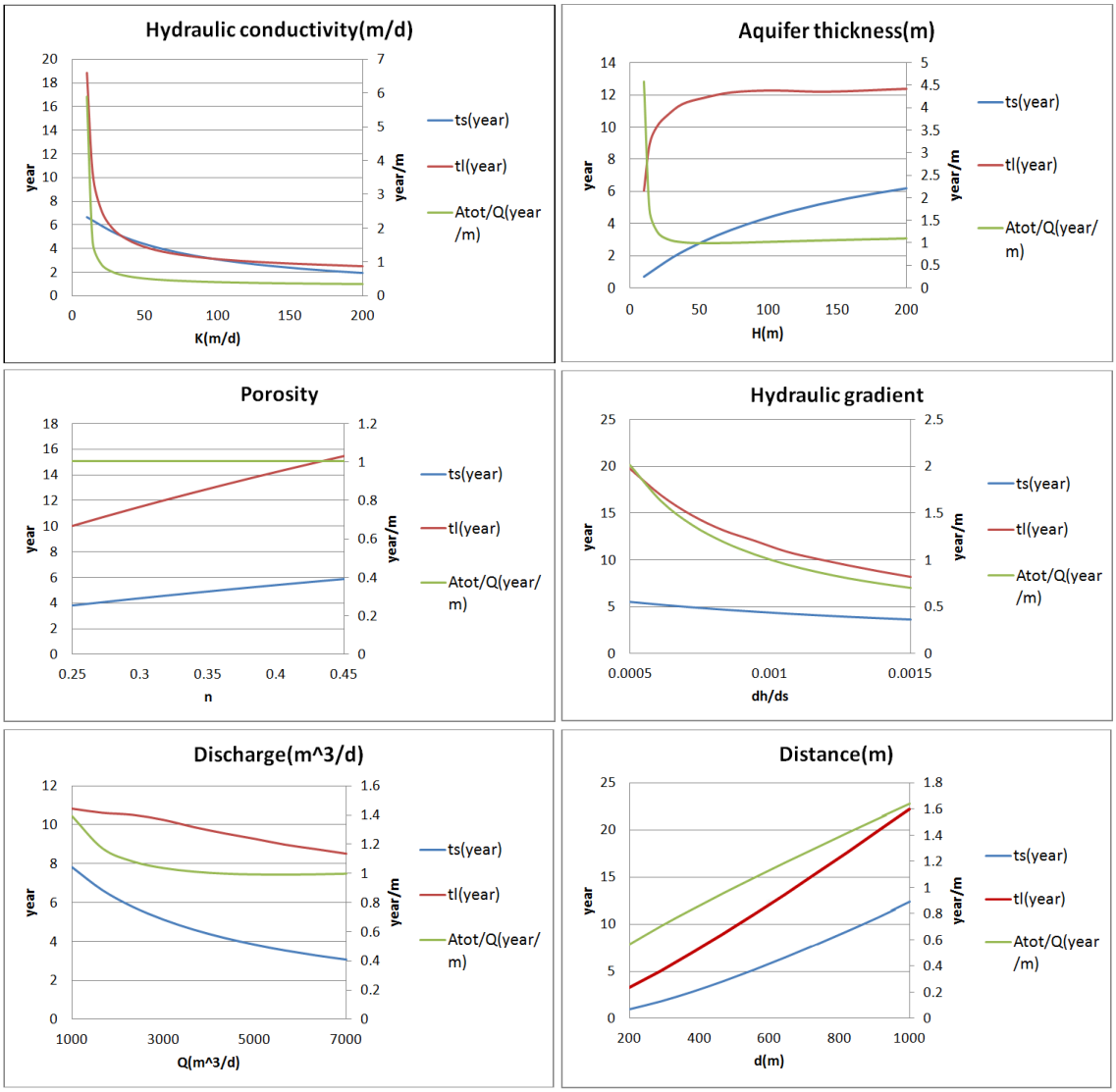

Figure 12. Criteria vs. different parameters

Hydraulic conductivity (K) is an essential parameter for system performance. It is difficult

to transport groundwater when K is a small number (< 10 m/d). With hydraulic conductivity increasing, the longest thermal travel time (t_l) and system total surface / injection well discharge (A_{tot}/Q) decreased dramatically, while the shortest thermal travel time (t_s) slowly decreased. The results showed that the ATEST system was sensitive with hydraulic conductivity, and a low K value seemed unrealistic.

With aquifer thickness (H) increasing, t_s rose slightly (from 1.5 years to 6.2 years), but t_l became steady when H was over 60m. A_{tot}/Q firstly reduced but then increased, and a low A_{tot}/Q value (high efficiency) was reached when aquifer thickness was about 50m. With high aquifer thickness, a decreasing gap was reached between the shortest and longest thermal travel time.

In the simulation, porosity (n) did not influence the shape of capture zone, and A_{tot}/Q stayed constant. However, for a capture zone with constant area and volume, increasing porosity meant more void space for groundwater, and, thus, the underground flow was lagged. With porosity increasing from 0.25 to 0.45, t_s shortened to 3.9 years from 6.0 years, and t_l reached 15.3 years from 10.0 years.

Hydraulic gradient (dh/ds) is an essential parameter that drives underground flow. In the simulation, t_l and A_{tot}/Q were affected by dh/ds dramatically, for, with the increase of dh/ds, these two criteria dropped inversely. Furthermore, with the hydraulic gradient increasing, the minimum thermal travel time slowly reduced from 5.9 years to 3.7 years.

Well discharge (Q) determines system capacity and influences system performance. With Q increasing, the underground flow accelerated, so t_s and t_l reduced from 7.9 to 3.1 years and 11.8 to 8.4 years respectively. Similar with aquifer thickness, with a larger well discharge, A_{tot}/Q firstly decreased and then increased, reaching the highest efficiency when $Q=5000m^3/d$.

A longer distance (d) indicates a greater transport capacity, but increasing transport time would make it more difficult to bound the capture zone. When transport distance lengthened from 200m to 1000m, all the criteria (t_s, t_l and A_{tot}/Q) quickly increased.

In summary, except for aquifer thickness (H) and well discharge (Q), other parameters have single-direction influence on system performance. Hydraulic conductivity (K), aquifer thickness (H) and hydraulic gradient (dh/ds) can strongly influence the ATEST system when they are in low values (thermal travel times and A_{tot}/Q), but these three parameters become decreasingly significant when they are in higher values.

4.2. Multi-influence on System performance

In this part, multiple influences surrounding hydraulic conductivity (K), aquifer thickness (H), well discharge (Q) and transport distance (d) are discussed. Two or three parameters are adjusted simultaneously, and results are shown in 3-D graphs.

Hydraulic conductivity

Low hydraulic conductivity is a common situation but is negative for heat transport. However, the negative effects of low hydraulic conductivity could be offset by low porosity, high hydraulic gradient or short transport distance.

Both hydraulic conductivity and hydraulic gradient have significant influence on system performance. The former depends on the aquifer's intrinsic permeability, while the latter drives the underground flow and bounds the capture zone. In principle, the ATEST system should work in the aquifer with high hydraulic conductivity and gradient. As shown in Figure 13, the thermal travel time doubles if both hydraulic conductivity and hydraulic gradient are large, while, with high K and dh/ds, A_{tot}/Q halves, which indicates less energy loss.

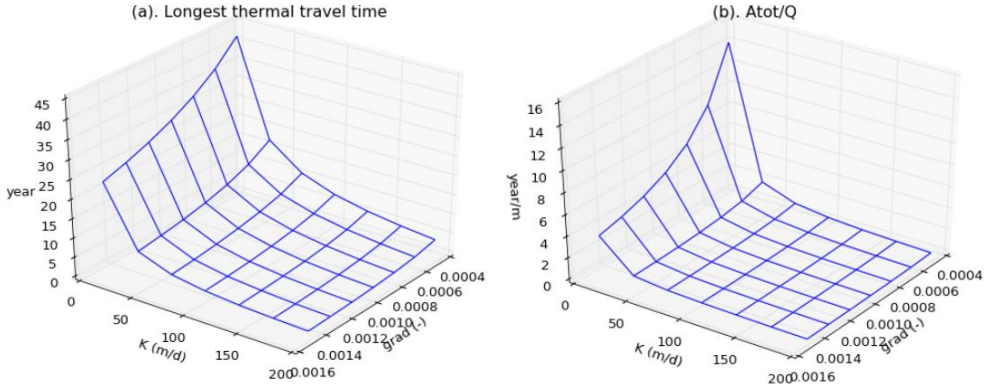

Figure 13. t_l and A_{tot}/Q vs. K and dh / ds

Lower porosity does not influence capture zone, but accelerates underground flow and reduce thermal travel time. Same as hydraulic conductivity, porosity is an inherent characteristic of aquifer. For underground flow, the promotion from low porosity may offset the lag from low hydraulic conductivity. Therefore, an aquifer with low hydraulic conductivity and low porosity may be useful, while one with high hydraulic conductivity and high porosity may be useless. Figure 14 shows the double influence from K and n. In both (a) and (b), the thermal travel time is approximately the same under the conditions of K=100m/d, n=0.25 and K=200m/d, n=0.45.

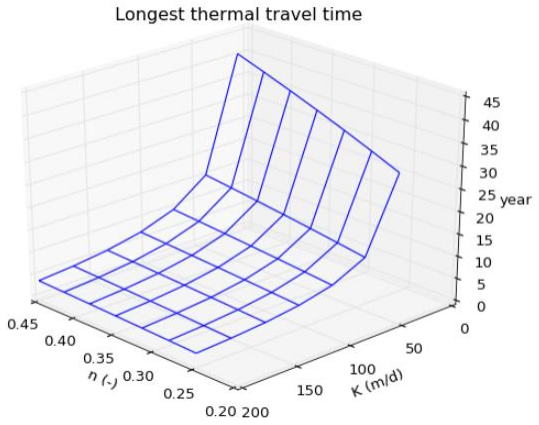

Figure 14. t_l vs. K and n

In practice, long transport distance is a main factor that increases thermal travel time. A system with short transport distance has lower requirement on hydraulic conductivity. Figure 15 shows the double effect from hydraulic conductivity and transport distance. It can be seen that, when d is 500m and K is 50m/d, the longest thermal travel time is about 15 years, which equals the result under the condition of d=1000m and K=100m/d. Furthermore, A_{tot}/Q quickly decreases with shorter transport distance and higher hydraulic conductivity.

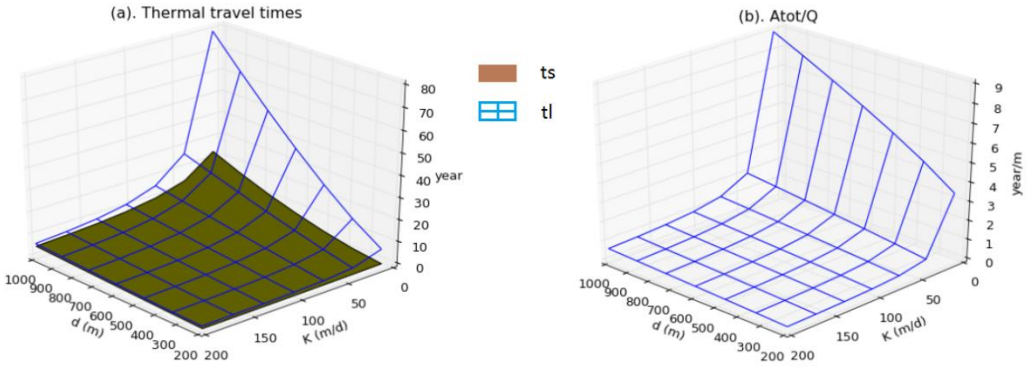

Figure 15. Criteria vs. K and well distance

Hydraulic conductivity and porosity are aquifer's inherent characteristics, but hydraulic gradient and transport distance can be controlled and selected. In general, the aquifer with high hydraulic conductivity and low porosity is more valuable for the ATEST system. Low hydraulic conductivity and high porosity have an adverse influence on system performance, which, however, could be offset by high hydraulic gradient and short transport distance.

To make the system valuable, in the analytical simulation, the longest thermal travel time should be limited within 20 years. As to results, hydraulic conductivity should not be lower than 20m/d, because it is costly to generate high hydraulic gradient and the aquifer with a hydraulic conductivity that is over 50m is valuable for the ATEST system.

High hydraulic conductivity and gradient reduce A_{tot}/Q, while porosity does not influence A_{tot}/Q at all. High hydraulic conductivity, high hydraulic gradient and low porosity promote underground flow and reduce thermal travel time. To build an ATEST system with high efficiency and short thermal travel time, a low porosity (<0.35) is required.

Aquifer thickness

Aquifer thickness significantly influences system efficiency, mainly by affecting the capture zone and changing the value of A_{tot}/Q. When the aquifer becomes thicker, A_{tot}/Q first decreases significantly, but then increases slightly once the optimal thickness is reached, indicating a larger heat loss,.

High hydraulic conductivity reduces thermal travel time, while thicker aquifer makes the shortest travel time longer, and these two opposite trends may be offset by each other. In Figure 16, (a) shows the shortest thermal travel time versus K and H, where the system quickly responses when hydraulic conductivity (>150m/d) is high, even with high thickness. In figure (b), under different hydraulic conductivities, A_{tot}/Q reaches its minimum in different aquifer thickness. Generally, the value of optimal aquifer thickness is lower when hydraulic conductivity is high.

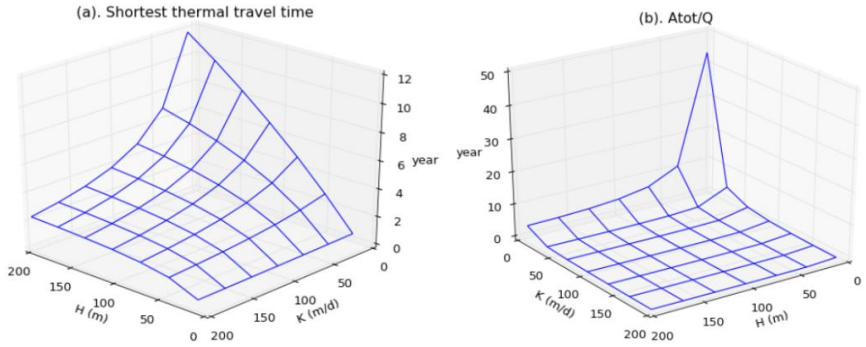

Figure 16. t_s and A_{tot}/Q vs. H and K

In Figure 17, the transport distance has a linear effect on system efficiency. The relationship between A_{tot}/Q and aquifer thickness does not change under any transport distance, indicating that aquifer thickness and transport distance are independent from each other.

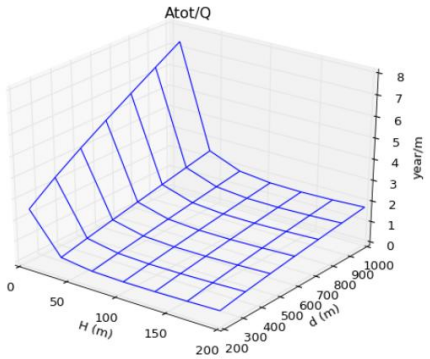

Figure 17. 'A_{tot}/Q' vs. 'H' and 'd'

In summary, when A_{tot}/Q reaches its minimum level, the aquifer thickness is optimal for system efficiency, but this optimal value varies with different hydraulic conductivities. In general, when H>60m, A_{tot}/Q changes slightly, so 60m is the minimum level allowed for aquifer thickness.

Well discharge and transport distance

Well discharge and transport distance determine system performance and system capacity. Long transport distance promotes the ATEST system's capacity, but increases the thermal travel time simultaneously, while well discharge reduces the thermal travel time, and maximizes the value of system efficiency.

Figure 18 shows the system performance with respect to transport distance and well discharge. With transport distance increasing, thermal travel time and A_{tot}/Q rise linearly. The highest system efficiency, or lowest A_{tot}/Q is reached when Q=4000m^3/d and d=200m. In principle, the well discharge needs to be determined as the optimal value or larger, and transport distance should be determined to be small.

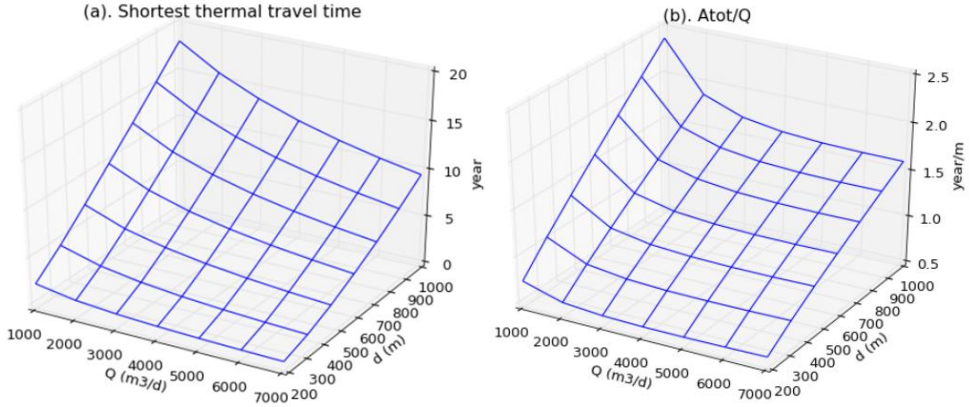

Figure 18. t_s and A_{tot}/Q vs. Q and distance

From Figure 19, it is known that thermal travel time is apparently affected by transport distance when dh/ds is low, and a high hydraulic gradient, which can decrease A_{tot}/Q, should be generated if the transport distance is long. To sum up, the hydraulic gradient should be determined together with the transport distance, so as to achieve the low hydraulic gradient required for a short distance, as in dh/ds=0.0005 for d=500m. However, high hydraulic gradient is necessary for a long distance, as in dh/ds=0.0015 for d =2,000m.

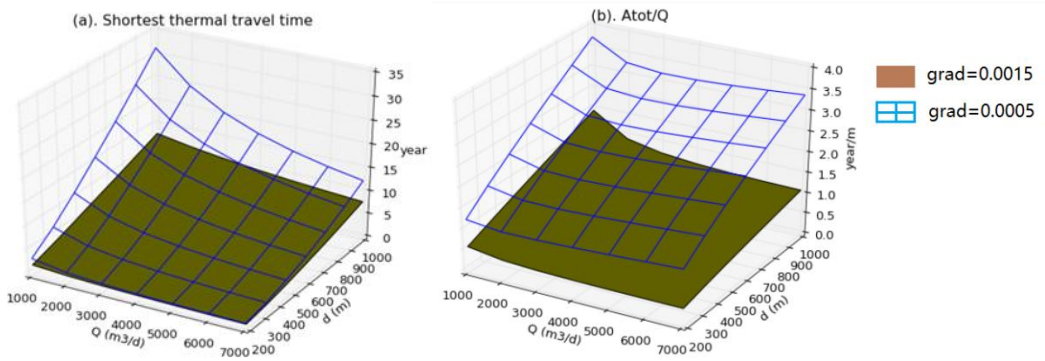

Figure 19. t_l and A_{tot}/Q vs. Q and d in different dh/ds

System with protection wells

The ATEST system, where K=50m/d, H=100m, n=0.3, Q=4,000m^3/d, and d=500m, worked with protection wells and under ambient underground flow respectively firstly, and then the profiles of water head were drawn. The protection wells (±200m, ±100m) were far from the injection and extraction wells with 4,000m^3/d. The hydraulic gradient from ambient underground flow was 0.001.

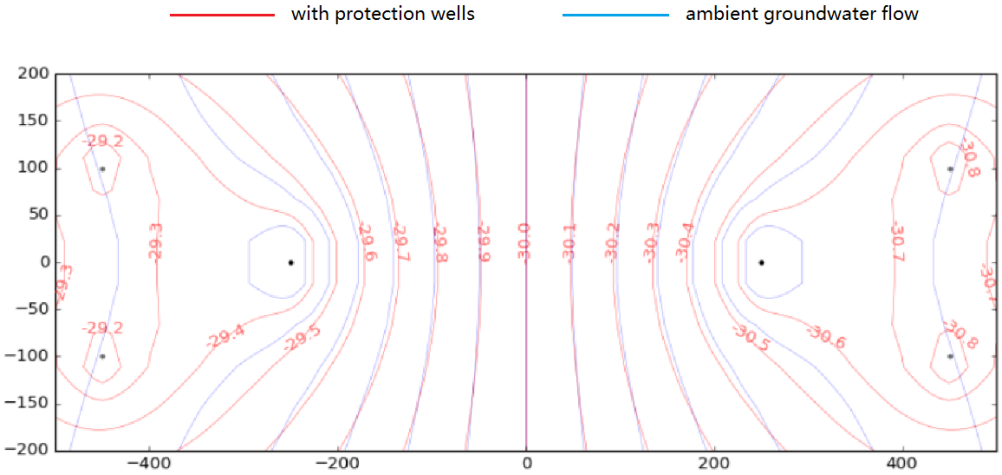

Figure 20. System water head profile

The discharge of protection well is the dominant factor that affects water head profile, while influences of the location and number of protection wells are trivial. In Figure 20, the protection wells in 4,000m^3/d have approximately equal effects when dh/ds=0.001. In the simulation, the artificial hydraulic gradient was approximately linear with the discharge of protection well, so the discharge of protection wells should be about 2,000m^3/d to masure sure dh/ds=0.0005.

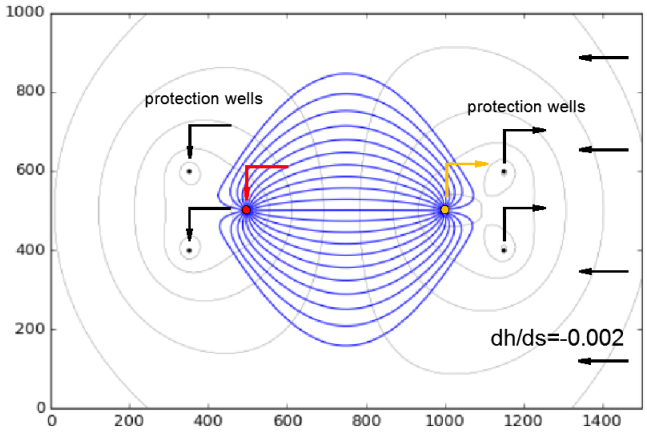

Figure 21. The ATEST system in negative ambient underground flow

In reality, the negative ambient underground flow should be overcome sometimes. As is shown in Figure 21, although the warm zone becomes wider with negative hydraulic gradient, the protection wells can effectively protect the warm zone from the background. However, the negative ambient hydraulic gradient should not be very large (e.g. should be >-0.002 when Q_{pro}=4,000m^3/d), otherwise the warm zone cannot be bounded and heat of the water will diffuse and disperse to the surroundings.

4.3. Summary

It can be identified that the analytical simulations within the bandwidth of working conditions specified in Table 2 are possible.

Table 2. Suitable geological and geo-hydrological conditions for ATEST

Hydraulic conductivity	20 – 150m/d
Aquifer thickness	30 – 120 m
Porosity	0.20 – 0.35
Hydraulic gradient	5×10^{-4}—1.5×10^{-3}
Distance between injection and extraction wells	200 – 1,000 m
Injection Well discharge	2,000-10,000 m^3/d

It is concluded that:

- Aquifers with K>50m/d (20°C) are valuable for the ATEST system, but the hydraulic conductivity could be lower due to the compensation from low porosity, high hydraulic gradient and high temperature.
- The system reaches the lowest A_{tot}/Q with specific aquifer thickness and injection

discharge. Generally, the conditions of H=60m and Q=4,000m^3/d are reasonable for the 500m transport distance.

- Thermal energy can be transported faster under low porosity, and the ATEST system has a good performance when the aquifer's n<0.35.
- Higher hydraulic gradient promotes underground flow and improves A_{tot}/Q simultaneously, for the basic model dh/ds=0.001 is rational.
- With longer transport distance, the thermal travel time is lagged and system efficiency decreases linearly.
- Small well discharge reduces system efficiency dramatically and shortens the thermal travel time. Thus, the ATEST system could be designed on a large scale, with Q>4,000m^3/d.
- Protection wells should be used when the groundwater is stagnant. Besides, the artificially created hydraulic gradient depends on the discharge of protection wells. If a negative ambient hydraulic gradient is present, but not too high (<0.002), protection wells may still create the required gradient.

5. Results from numerical simulations

15 scenarios were studied in the numerical simulation. The models were tested with different intrinsic permeability (k), aquifer thickness (H), well discharge (Q and Q_{pro}) and transport distance (d). The scenarios are summarized in Table 3. The porosity (n) is constant and the hydraulic gradient (dh/ds) is 0.001 when there are no protection wells (Q_{pro}=0).

Table 3. Scenarios

Scenarios	k(m^2)	H(m)	n(-)	Q(m^3/d)	Q_{pro}(m^3/d)	d(m)	dh/ds
01	3e-11	30	0.35	8000	6000	500	0
02	**1.5e-11**	30	0.35	8000	6000	500	0
03	**6e-11**	30	0.35	8000	6000	500	0
04	3e-11	**15**	0.35	8000	6000	500	0
05	3e-11	**60**	0.35	8000	6000	500	0
06	3e-11	**120**	0.35	8000	6000	500	0
07	3e-11	30	0.35	**4000**	6000	500	0
08	3e-11	30	0.35	**12000**	6000	500	0
09	3e-11	30	0.35	**16000**	6000	500	0
10	3e-11	60	0.35	8000	**4000**	500	0
11	3e-11	30	0.35	8000	**8000**	500	0
12	3e-11	30	0.35	8000	**0**	500	**0.001**
13	3e-11	30	0.35	8000	6000	**100**	0
14	3e-11	30	0.35	8000	6000	**250**	0
15	3e-11	30	0.35	8000	6000	**1000**	0

Additionally, analytical simulations were executed based on these 15 scenarios, to assist analyzing numerical simulations.

5.1. Results and analysis

5.1.1. Heat transport process

The heat transport process can be understood by tracing the temperature profile. In this part, the ATEST system in scenario 01 was studied. The aquifer for heat transport was 51-81m underground, confined by one 50m-thick leaky layer above and one 20m-thick leaky layer below.

The injected hot water was promoted by the injected protection wells. It can be seen in Figure 22 that 0.75 years after the injection well started to operate the warm water reached the extraction well. From then on, increasing warmer water can be extracted. Vertically, the heat conduction was obvious, but the heat was still mainly confined in the aquifer layer.

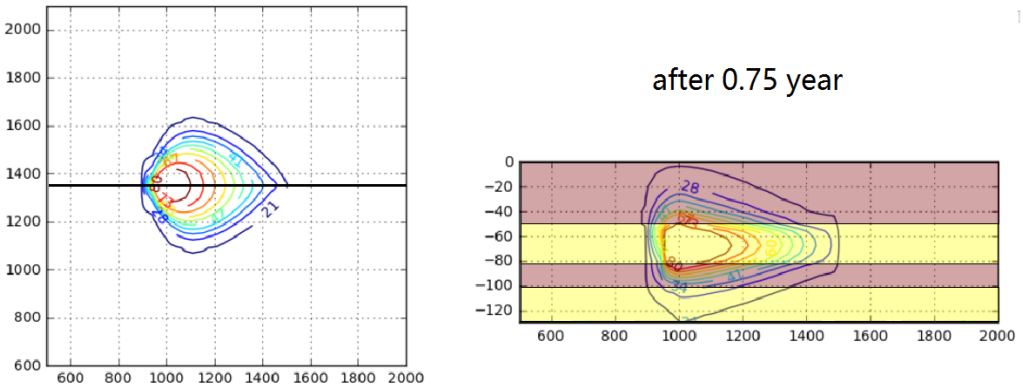

Figure 22. Temperature profile after 0.75 years

According to Figure 23, between 0.75-3 years, the temperature of extracted water quickly increased (>12°C/year), while, after 3 years, the increase became slower (about 1°C/year). Vertically, the heat seriously permeated into confining layers. The heat rises to ground surface, and sinks due to the driven force from deeper supplementary wells. In result, heat starts losing at ground surface and being extracted by supplementary wells. Further from the injection well the heat loses in slower speed. Vertically, the density driven flow can be observed because the upper confining layer was more seriously heated.

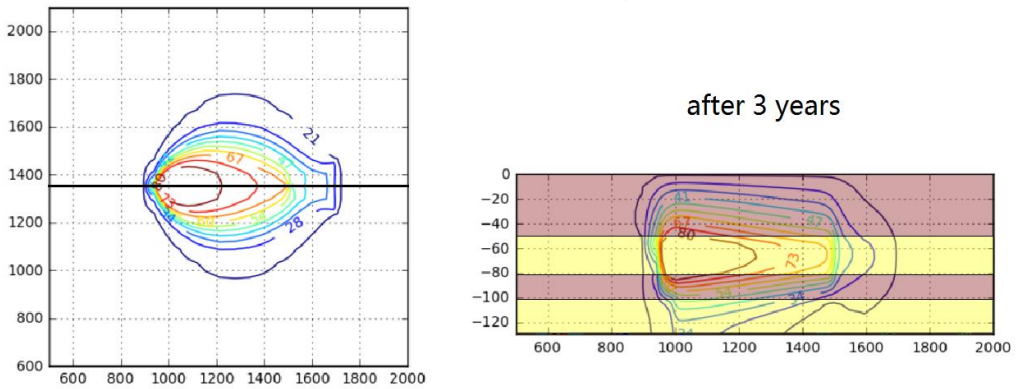

Figure 23. Temperature profile after 3 years

As can be seen in Figure 24, after 5 years, the system became more steady, although the water temperature kept increasing slowly at the extraction well (<0.5°C / year). The area of the warm zone did not increase, but the temperature profile continued changing. The whole upper leaky layer was heated inside the warm zone, especially at the injection

well, and much heat diffused to the lower aquifer and was then extracted by supplementary well. It was inferred the heat was lost in three ways: 1) extracted by the extracted protection wells as warm water, 2) lost at the ground surface by heat diffusion and density driven flow, and 3) diffused to deeper underground and finally extracted by the supplementary wells. In scenario 01, about 15.3% heat loss occurred at the extracted protection wells, which could be reused in practice.

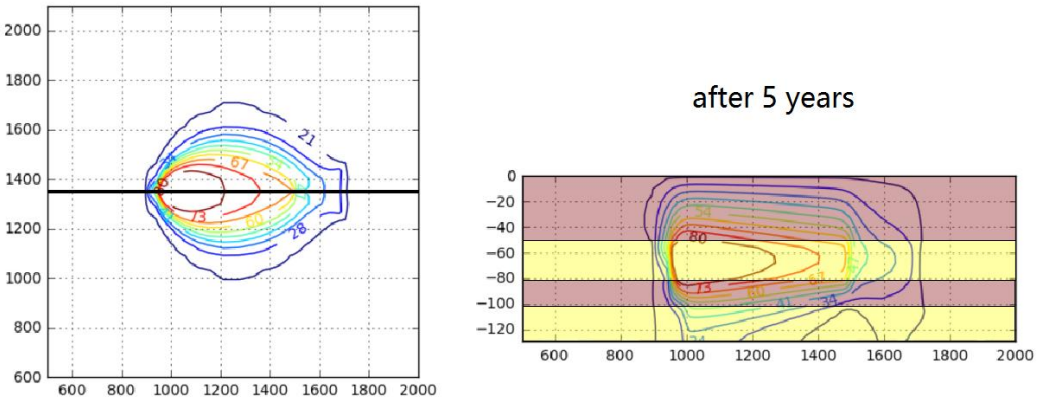

Figure 24. Temperature profile after 5 years

According to Figure 25, after, the system worked stably. In scenario 01, the warm zone was in a roughly circular shape, which was between the injection well and the extracted protection wells in x axis, and about ± 400m in y axis. Vertically, the heat was mainly transported downward, causing about 47.8% heat loss, and finally extracted by the supplementary wells, and 36.9% heat loss occurs at the ground surface. In the upper leaky layer, the vertical temperature slope was about 1.3°C/m at the injection well, which could pose some practical problems for ground use.

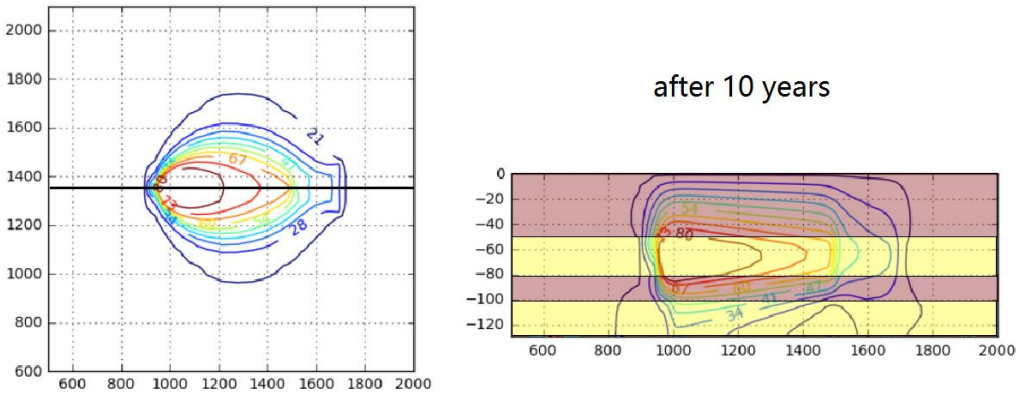

Figure 25. Temperature profile after 10 years

5.1.2. Results and sensitivity analysis

System performances are summarized in Table 4 below.

Table 4. System performance of 15 scenarios

Scenarios	ts(years)	tl(years)	eff.(%)	int. eff.(%)
01(d=500m, basic)	0.63	1.88	60.00	55.10
02(k=1.5×10^{-11}m^2)	0.63	1.88	60.44	55.33
03(k=6×10^{-11}m^2)	0.63	1.88	58.35	53.40
04(H=15m)	0.50	1.58	51.89	48.49
05(H=60m)	0.92	2.50	63.64	56.25
06(H=120m)	1.67	4.25	62.86	50.12
07(Q=4000m^3)	0.75	2.25	48.11	43.17
08(Q=12000m^3)	0.42	1.75	64.23	59.36
09(Q=16000m^3)	0.33	1.58	66.50	62.32
10(Q_{pro}=4000m^3)	0.67	2.50	54.88	49.31
11(Q_{pro}=8000m^3)	0.50	1.50	60.74	56.67
12(Q_{pro}=0, dh/ds=0.001)	0.83	3.75	35.82	30.55
13(d=100m)	0.08	0.17	82.37	81.42
14(d=250m)	0.17	0.67	72.63	70.39
15(d=1000m, Q=8000m^3/d)	3.75	8.67	30.56	17.37

Permeability

Scenarios 01, 02 and 03 have the same properties except for the intrinsic permeability. In Figure 26, it is shown that the intrinsic permeability does not have any influence on the thermal travel times. When the system is driven by artificial hydraulic gradient, main wells and protection wells are simultaneously influenced by the intrinsic permeability. Although warm water can be easily transported with high permeability, the artificial hydraulic gradient from protection wells is weakened.

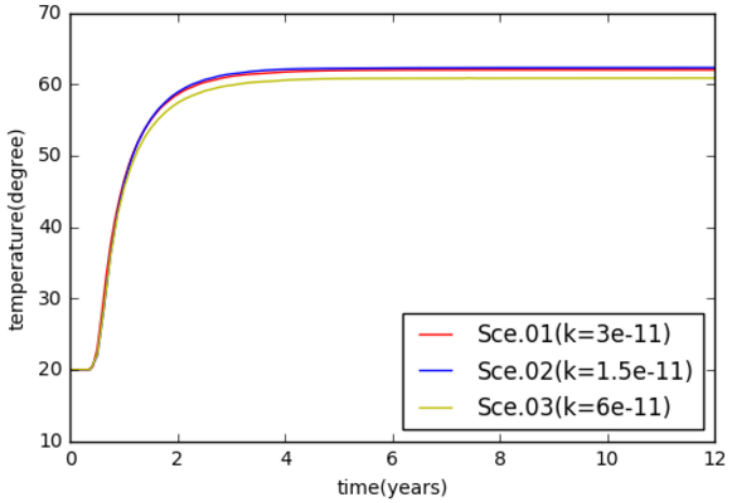

Figure 26. Temperature at the extraction well in scenarios 01, 02 and 03

However, the system efficiency decreases with higher intrinsic permeability. During the transport process, heat is continuously lost at the system boundary through convection, which is determined by the equation below:

$$Q = hA(T_s - T_l) \quad \ldots \quad 23$$

where h is the heat convection coefficient [W/s•m^2•°C], A is the surface area [m^2], T_s is the temperature of solid [°C], and T_l is the temperature of liquid [°C]. The convection coefficient h increases with higher intrinsic permeability, therefore, there will be more heat losses through the thermal convection at the system boundary, decreasing the system efficiency.

Aquifer thickness

By comparing scenarios 01, 04, 05 and 06, the influence of aquifer thickness can be identified, that is, the results from numerical models are highly consistent with the results from analytical models. In Figure 27, the system efficiency reaches the top when H=60m, and then the system efficiency reduces no matter the aquifer becomes thinner or thicker. However, the thermal travel times are longer in thicker aquifers, which may reduce the integral system efficiency. As a result, the final efficiency is highest when H=60m, but the integral efficiency is highest when H=30m.

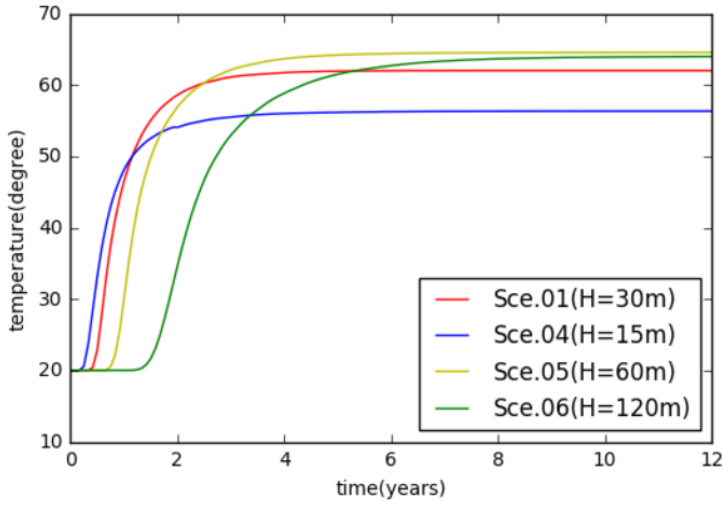

Figure 27. Temperature at the extraction well in scenarios 01, 04, 05 and 06

Figure 28 shows the vertical profile of temperature with different aquifer thicknesses. When the aquifer is too thin, the ATEST system can still achieve the transport function but the heat loss accelerates because the heat storage is low. When the aquifer is too thick, more heat losses occur due to the conductivity because: 1) it takes the warm a longer time to be exposed to surroundings before the extraction, and 2) the warm zone and A_{tot}/Q are larger.

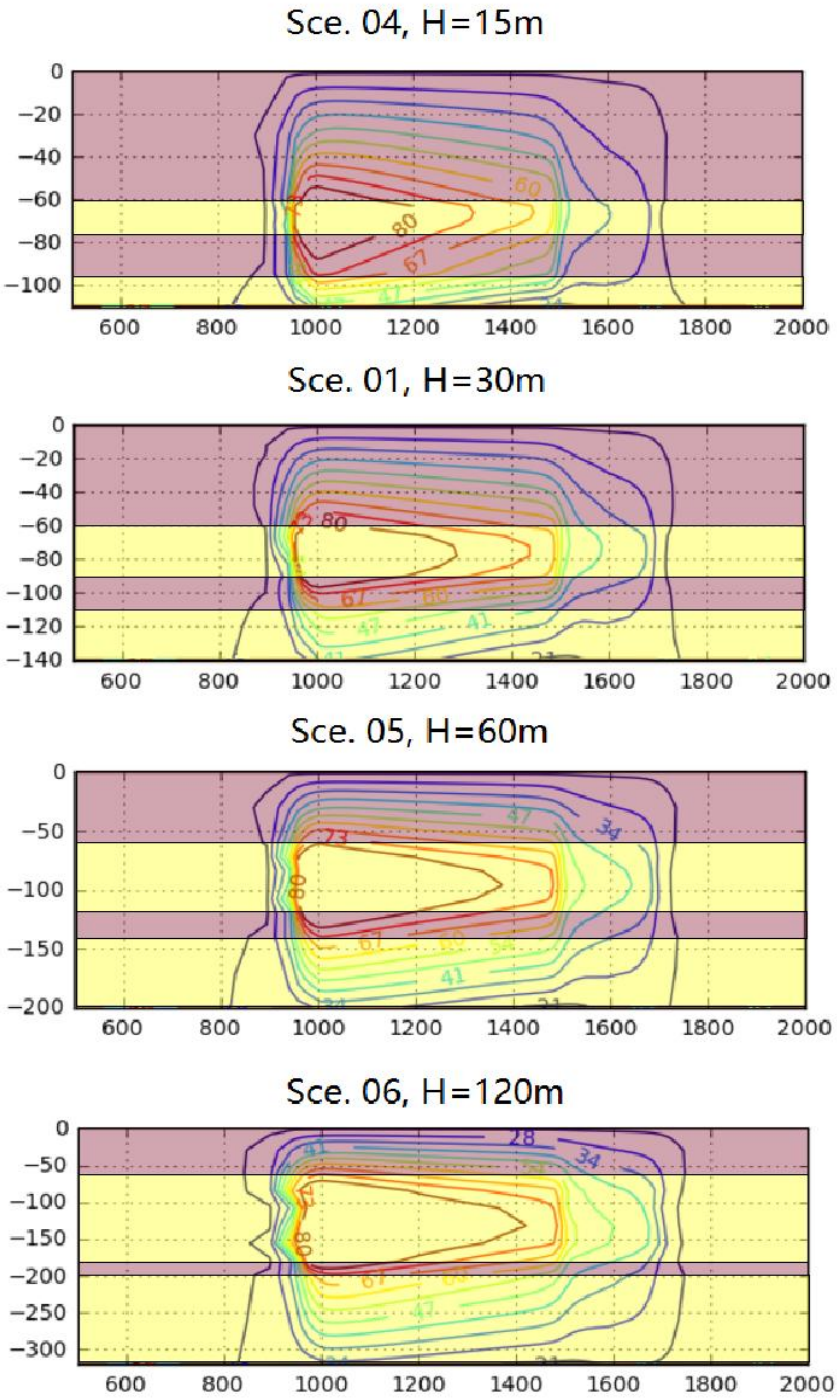

Figure 28. Vertical temperature profile under steady conditions when d=500m

Due to the density driven flow, warm water tends to flow upward, but the supplementary wells generate hydraulic gradient vertically, which makes the warm water tend to flow downward. These two counteractions cause about equal amounts of heat losses in the two directions.

Discharge of injection & extraction wells

In Figure 29, the system performance improves dramatically with increasing well discharge. In this scenario, both system efficiency and thermal travel time reach the top when Q=16,000m^3 / d, and the system performance is worst when Q=4,000m^3 / d.

The system was tested at the rate of 4,000m^3/d increase per step. However, the system performance increases not linearly, but inversely, with the biggest improvement achieved from Q=4,000m^3/d to Q=8,000m^3/d. The numerical models show that the ATEST system is supposed to meet large heat demand. For example, the heat demand is supposed to be larger than 8000m^3/d when the transport distance is 500m.

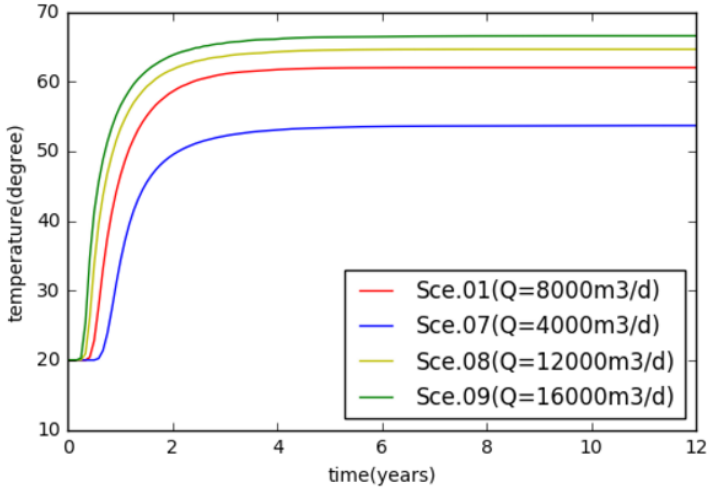

Figure 29. Temperature at the extraction well in scenarios 01, 07, 08 and 09

Generally, the area of warm zone is larger with increasing well discharge, which may have some adverse effects on land use. This phenomenon should be considered in practice.

Discharge of protection wells

When the system is working, cold water continues to be injected by the injected protection wells to drive warm water to the extraction well. Larger discharge of protection wells gives the system larger driving force to promote the transport process and bound the warm zone into a smaller area, which reduces the heat conduction and improves system efficiency. Additionally, when the discharge of the protection wells is larger, the stronger convection at the boundary of warm zone increases the heat loss to the extracted protection wells and raises the temperature there.

In practice, the warm water from the extracted protection wells may be used, so the heat extracted by the protection wells may be not considered as part of the heat loss, and the system efficiency can be further improved when the discharge of protection wells grows.

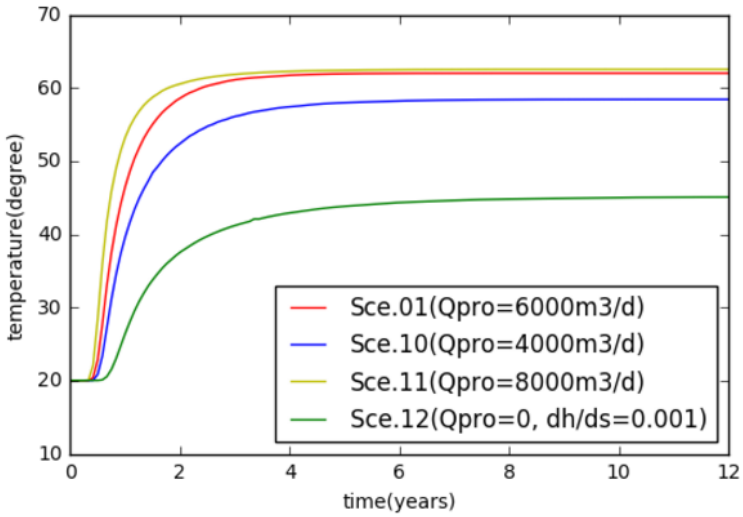

Figure 30. Temperature at the extraction well in scenarios 01, 07, 08 and 09

Transport distance

It is shown in Figure 31 that the transport distance is the dominant parameter for system performance.

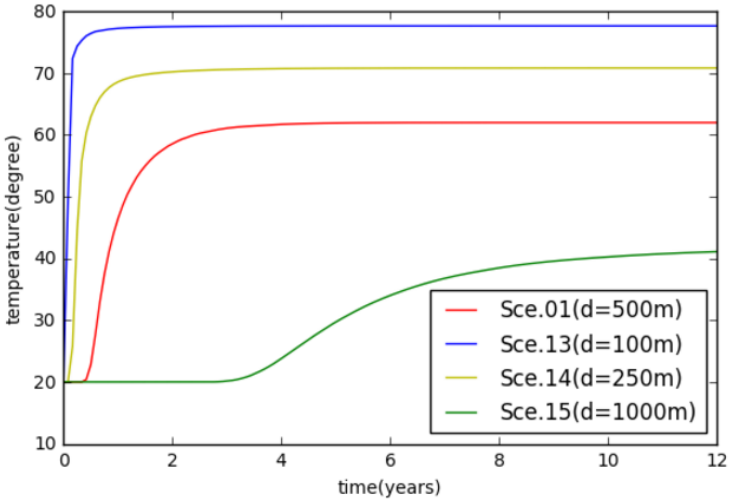

Figure 31. Temperature at extraction well in scenario 01, 13, 14 and 15

Thermal travel times are linearly influenced by transport distance when d≤500m, but the system needs a very long time to extract hot water if the transport distance is too long. Compared with scenario 01, the transport distance in scenario 15 is doubled, but the shortest thermal travel time (t_s) is 6 times longer and the longest thermal travel time (t_l) is 4.6 times longer. As is shown in Figure 32, the warm zone enlarges quickly with longer transport distance, and the retardation becomes more obvious because much more warm water is stored in the aquifer and lost through conduction.

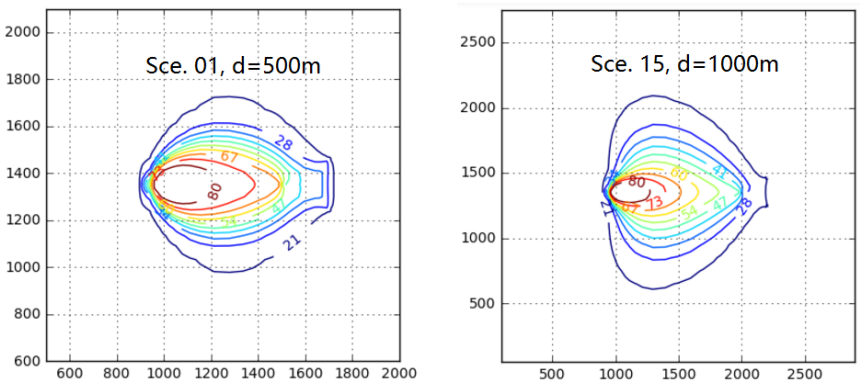

Figure 32. Warm zone in different transport distances

The system efficiency dramatically decreases when transport distance lengthens. With a shorter transport distance, the heat loss is reduced in two ways: 1) the warm water's time to be exposed to surroundings before the extraction is shorter, reducing the time of thermal conductivity, and 2) the warm zone is much smaller, limiting the space of the thermal conductivity.

In conclusion, ATEST is not useful for transporting heat in a long distance. Generally, the system has an outstanding performance when d≤500m, and high system efficiency (>70%) can be achieved if d≤250m.

5.1.3. Comparison with analytical analysis

Due to the different methods in the simulations, the results from the numerical models are somewhat different from those from the analytical models.

Shortest thermal travel time

Figure 33 shows the shortest thermal travel time from the analytical and numerical simulations between the correlation value ρ=0.841 and T-test value T=0.907. Therefore, the results from different simulations are matched. Although the two data groups change in the same tendency, large deviations exist in scenarios 05, 06 and 15. In scenarios 05 and 06, the aquifer thicknesses are enlarged, and the deviation is larger when H=120m. This was caused mainly by the density driven flow. When the aquifer was thin, the advection was the main process in transport, while the density driven flow (by temperature difference) is more obvious when the aquifer is thick. Besides, the transport was driven at the upper part of the aquifer. Therefore, the thermal travel times were overestimated in the analytical models. In scenario 15, the warm zone is much larger due to the longer transport distance, which amplifies the retardation and makes the numerical results larger.

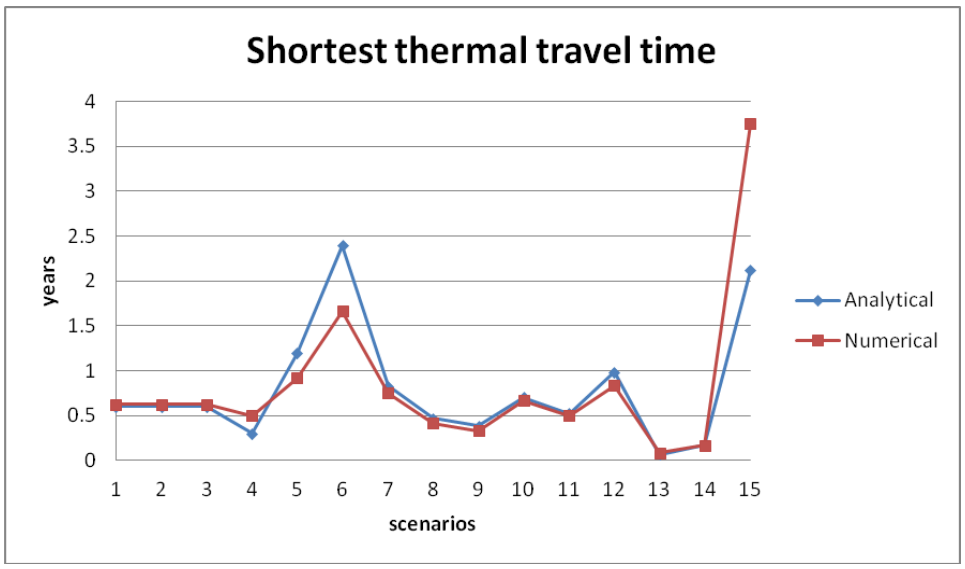

Figure 33. T_s of 15 scenarios in the analytical and numerical models

Longest thermal travel time

Compared with t_s, t_l of the analytical and numerical simulations were the least consistent. The correlation between these two groups was 0.832, and T=0.193. Generally, the numerical results are higher, but when the aquifer is thick (H=60 and H=120m), the deviations are smaller. In the analytical simulations, the traced particles did not have the longest travel route or travel time, so the results were generally underestimated. In figure 34 (a), if the results of the analytical simulations are multiplied by 1.8, as is seen in Figure 34 (b), the analytical and numerical results will be much better matched (T=0.553), like those in Figure 33.

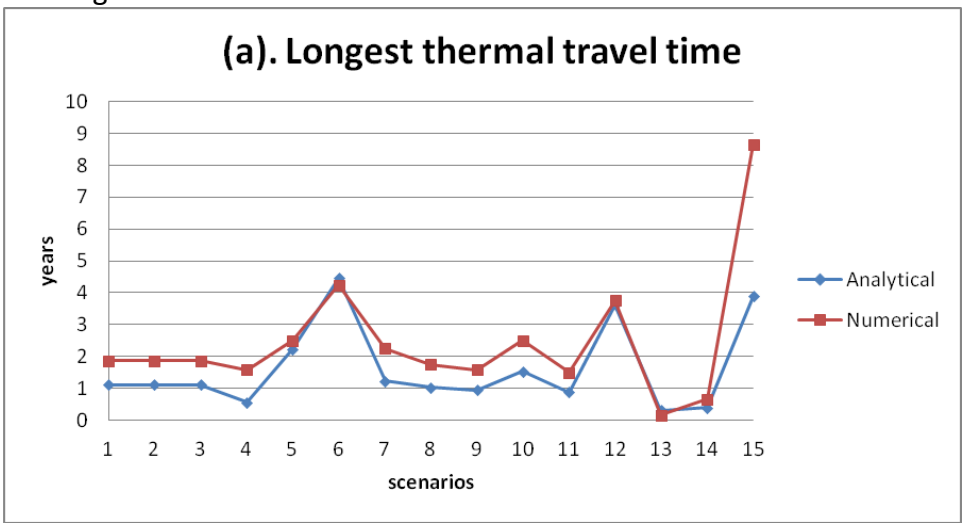

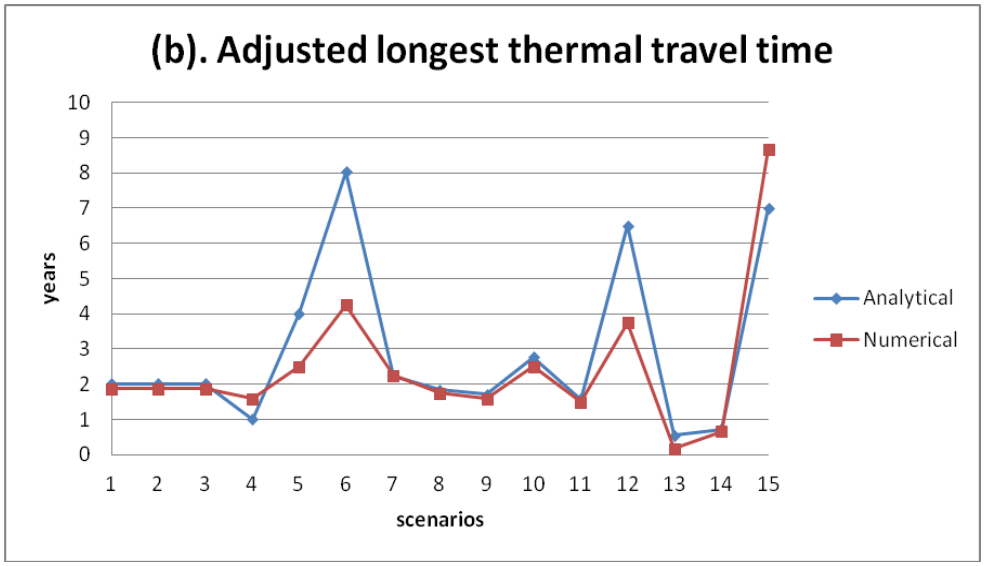

Figure 34. T_l and adjusted t_l for 15 scenarios in the analytical and numerical models

A_{tot} / Q with efficiency

Based on the results from 15 scenarios, A_{tot} / Q can be proved to be properly related to system efficiency. Figure 35 shows the comparison between A_{tot} / Q and η, and the correlation between these two indexes is ρ=-0.765.

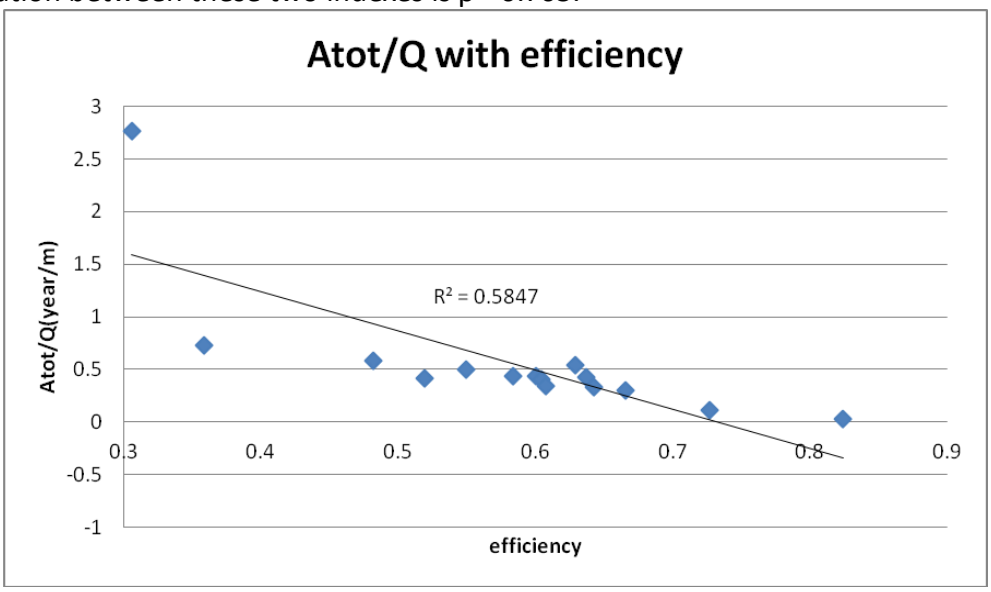

Figure 35. Comparison of system efficiency and A_{tot} / Q

5.2. Summary

In the numerical simulation, heat transport process was apparently affected by the thermal conduction. The warm water could be transported to the extraction well within a short time, but it took the ATEST system a long time to reach steady conditions. In the transport process, there were three ways of heat loss: 1) extracted by the extracted protection wells (15-30%), 2) lost at the ground surface (25-40%), and 3) diffused to the deeper underground (40-50%). The heat from extracted protection wells might be useful in practice.

It has been concluded that:

- Intrinsic permeability does not have an obvious influence on system performance.
- System reaches best performance in a specific aquifer thickness. When the aquifer is thin, the storage capacity of the ATEST system is small and heat is seriously lost through conduction, while the transport process is lagged and the thermal conduction is lengthened when the aquifer is too thick.
- The ATEST system has a better performance in meeting large heat demand, and the discharge of the injection & extraction wells should not be too low. And the heat demand does not have to be very large because system efficiency increases inversely with wells' discharge.
- A larger discharge of the protection wells will slightly reduce thermal travel times and increase system efficiency.
- The ATEST system cannot be used when the transport distance is too long. Generally, 500m is the maximum distance, and water should be transported within 250m to ensure high efficiency of the system.

The results from the analytical and numerical analyses were strongly correlative, but in some specific scenarios, the results were obviously different. When the aquifer was thick, the thermal travel times are overestimated under the ideal conditions (analytical simulation). However, in the analytical simulations, the t_l was mostly underestimated. If the t_l values from the analytical simulations had been amplified, the relationship between t_s and t_l would have followed the same pattern. In addition, A_{tot}/Q was proved to be useful in indicating system efficiency through the numerical simulations.

6. Case simulation

6.1. Material and method

6.1.1. Study area

In this chapter, an ATEST system was simulated in TU Delft, which already has a combined heat and power plant and is planning to develop a geothermal mining well. During summer, TU Delft has a heat surplus, which can be transported to serve the surrounding residential areas. The area of the experiment is located in Southwest TU Delft, near the Schie canal, and separated from the university campus, because the canal makes it costly to construct pipelines under the riverbed and transport warm water across. Selection of this area solved both the transport and storage problems for the ATEST system because heat is available in summer, while demand is in winter.

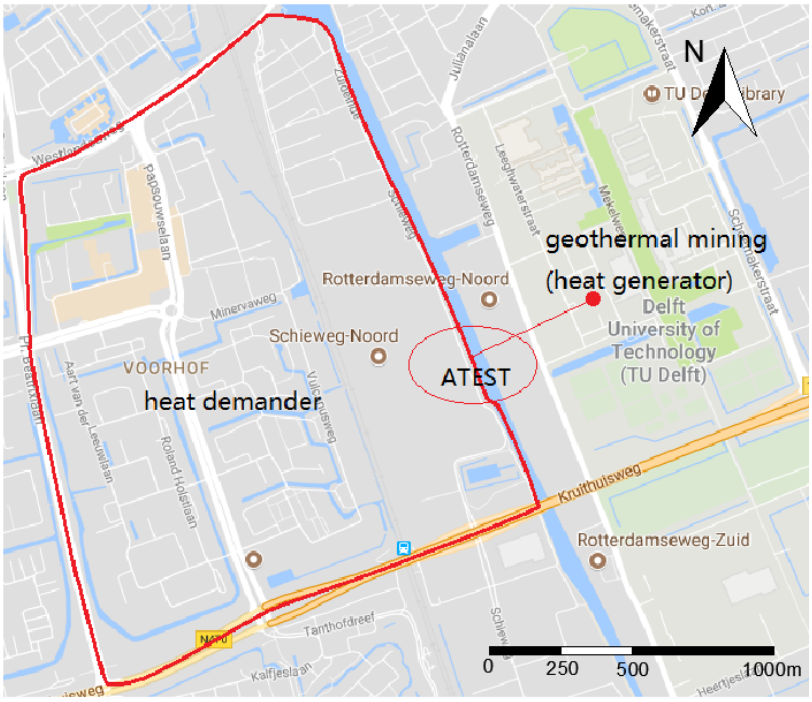

Figure 36. The layout of the case simulation area

Figure 36 shows the layout of the case simulation area, where the heat users are about 400m from the geothermal mining and CHP, and the canal is about 20m wide. There are about 15,000 current residents in the target area, accounting for a yearly heating demand of about 1.5×10^5 MWh. Although heat demands are various around the year, the heat generation is relatively constant. As a result, 4,000m^3/d of hot water at 90°C is constantly in store every day. And the injection well discharge should be >4,000m^3/d because of large heat losses during the transport process.

6.1.2. Geological data

The subsurface structure can be learned through the geological boreholes. In the target area, two aquifers are confined by three clay layers in the shallow underground space, qualifying for the system structure. The upper aquifer is 14m thick and lower aquifer is 23m, making them suitable for heat transport. In operation, the lower aquifer is used for heat transport, and the upper aquifer is for water balance. The lithology of the target area is shown in Figure 37.

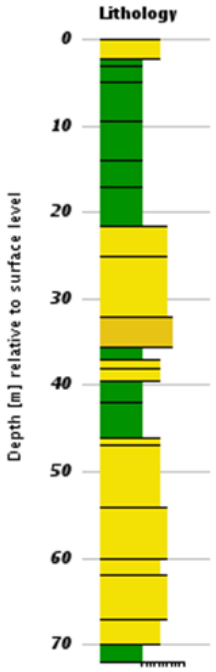

Clay
Sand, medium category
Sand, coarse category

	Type	Hydraulic conductivity (m/s at 20°C)	Porosity
0-2m	Sand, medium fine	1e-5	0.29~0.46
2-21m	Clay	5e-10~5e-8	0.29~0.41
21-25m	Sand, medium coarse	2.55e-5~5.35e-4	0.26~0.43
25-32m	Sand, medium coarse	2.55e-5~5.35e-4	0.26~0.43
32-35m	Sand, very coarse	2.55e-5~5.35e-4	0.26~0.43
35-37m	Clay	5e-10~5e-8	0.29~0.41
37-38m	Sand, medium fine	1e-5	0.29~0.46
30-47m	Clay	5e-10~5e-8	0.29~0.41
47-62m	Sand, medium fine	1e-5	0.29~0.46
62-67m	Sand, medium coarse	2.55e-5~5.35e-4	0.26~0.43
67-70m	Sand, medium fine	1e-5	0.29~0.46
>70m	Clay	5e-10~5e-8	0.29~0.41

Figure 37. Lithology of the target area[5][6]

6.1.3. Model description

This case simulation was done using the numerical model. The distance between the injection and extraction wells was 250m, while the injected protection wells were (-100, ±50) far from the injection well. To reduce the heat loss at the extracted protection wells, these two wells were (250, ±50) far from the extraction well. Vertically the subsurface is divided by 24 layers. The top layer represented ground surface, with the temperature set in periodic cycles, and the upper confining layer divided into five sub-layers of 4m, 4m, 4m, 4m, and 3m in thickness. The upper aquifer was the main layer in the ATEST system, divided by seven 2m-thick sub-layers. The lower confining layer included two clay layers

[5]. https://www.dinoloket.nl/en/subsurface-data
[6]. http://www.geotechdata.info

and one thin aquifer. The total thickness of the five layers was 12m. The lower aquifer was used for supplementing water, which was divided into five layers of 5m, 5m, 5m, 5m, and 3m in thickness. Below the lower aquifer was a thick (30m) confining layer serving as the system bottom.

The discharges of the injection well (4,000m^3/d) and injected protection wells (3,000m^3/d) were constant, while the discharges of the extraction well and extracted protection wells were periodic. In the basic simulation, the annual discharge of the injection well equaled that of the extraction well, and so did the discharges of the injected and extracted protection wells. The discharges of all the wells as well as the temperature at the ground surface are shown in Figure 38. In this chapter, the system efficiency is calculated by the equation 22, while the final efficiency can be calculated by an integral for the last year.

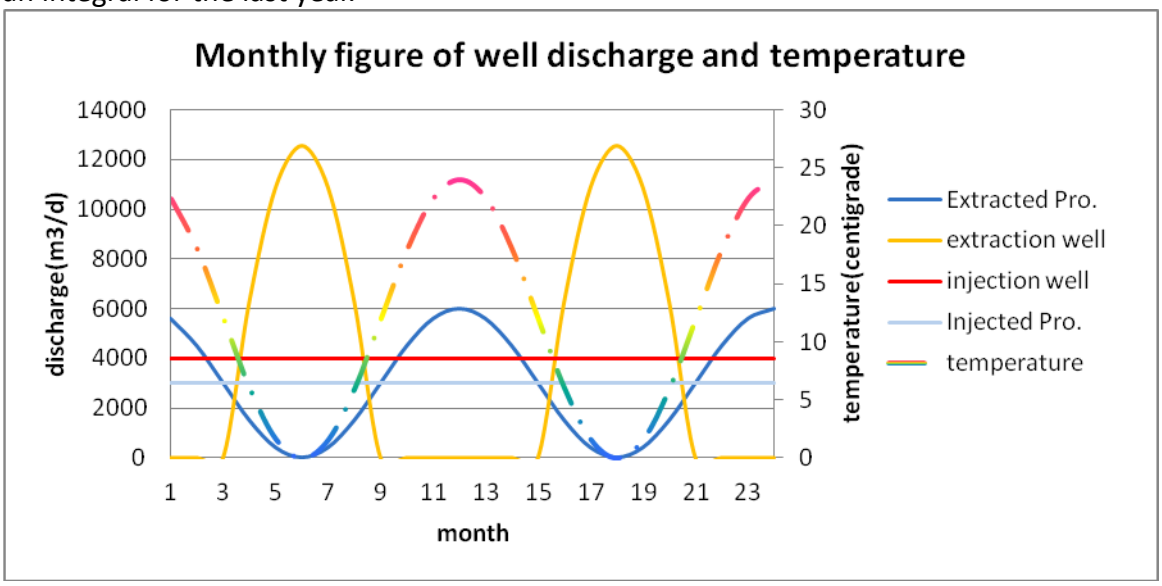

Figure 38. Monthly discharge of wells and air temperature

In the model, the porosity was set at 0.35, but the hydraulic conductivity was different in each layer: 5e-9m/s for clay, 5e-5m/s for fine sand, 2e-4m/s for medium sand, and 4e-4m/s for coarse sand. In operation, the system was tested in different extraction discharges and injection temperatures to study the influences of these two controlling parameters. The working conditions of 5 scenarios are summarized in the table below.

Table 5. Scenarios for case simulation

Scenarios	**$Q_{injection}$ (m^3/d)**	**Annual $Q_{injection}$/ Annual $Q_{extraction}$**	**$T_{injection}$ (°C)**
Case simulation 01	4,000	0.75	90
Case simulation 02	4,000	1	90
Case simulation 03	4,000	1.25	90
Case simulation (50°C)	8,000	1	50
Case simulation (70°C)	5,333	1	70

6.2. Results

6.2.1. Transport process

In this part, the ATEST system working in case simulation Sce.02 is studied.

The shape of the warm zone does not stay the same, because the discharges of the extraction well and extracted protection wells are not constant throughout the year. As is shown in Figure 39, in summer, the warm zone is enlarged because the extraction well is closed and only a limited amount of heat is extracted by the extracted protection wells, while, in winter, the warm zone shrinks because the extraction well is opened and more heat is extracted than injected due to $Q_{extraction} >> Q_{injection}$.

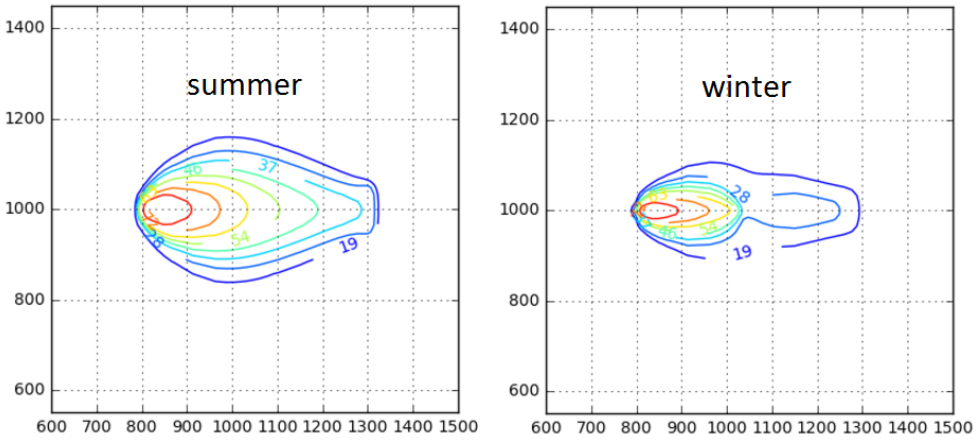

Figure 39. Temperature profile in different seasons

Figure 40 shows the temperature at the extraction well. In summer, warm water is stored in the ATEST system, expanding the warm zone and continuously increasing the temperature at the extraction well, while, in winter, more heat is extracted than injected, resulting in a decreasing temperature at the extraction well. In the heat-storing period (summer) the temperature at the extraction well rises negatively. It is shown in case simulation Sce.02 that the system works under a good condition; the system performance will reduce if the extraction well opens earlier or later.

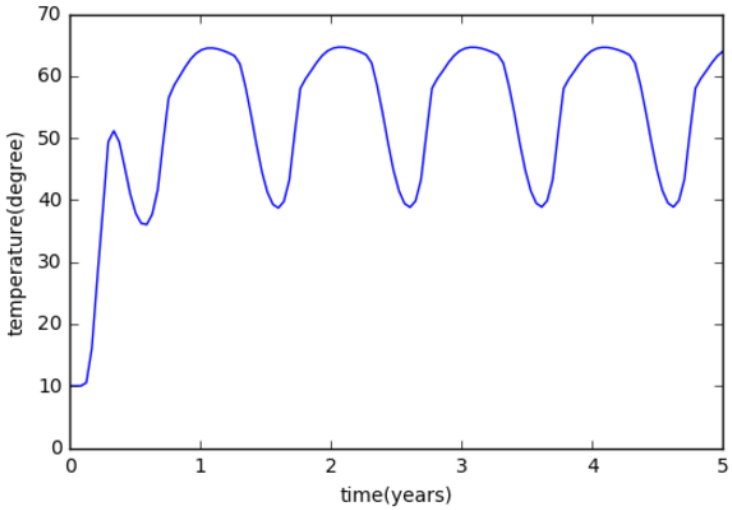

Figure 40. Temperature at the extraction well (case simulation Sce.02)

6.2.2. System performance

The system was tested with different extraction well discharges, and the results are summarized in Table 6. It can be seen that a larger extraction discharge improves system efficiency.

Table 6. System performance in different extraction well discharges

Scenarios	Final eff. (%)	Heat loss in extracting Pro (%)	Heat loss in supplementary wells (%)
Case simulation 01	42.28	9.41	17.96
Case simulation 02	53.72	7.28	15.45
Case simulation 03	63.31	6.35	13.63

From Figure 41, it can be learned that the value of $Q_{extraction}/Q_{injection}$ is not a key determinant of the peak temperature at the extraction well. Instead, it mainly influences the minimum temperature. With a larger discharge at the extraction well, the extracted warm water is in a low temperature and the thermal energy is in a low quality at the end of the annual operation, although more heat can be recovered and system efficiency can be improved.

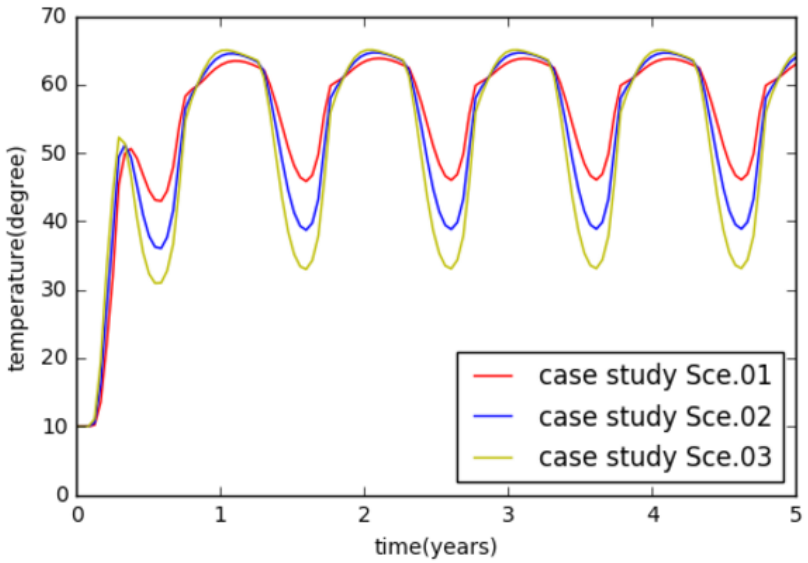

Figure 41. Temperature at the extraction well in different case simulation scenarios

The injection and extraction discharge should be larger to meet the heat requirement because less heat can be stored in the water with a lower temperature (50°C, 70°C), changing the transport process and system performance at the same time. Because thermal conduction at the system boundary is limited and the transport process is promoted, system efficiency obviously increases with lower injection temperature and larger discharge of wells. The system performances at different injection temperatures are summarized in Table 7. It can be seen that the heat loss through the extracted protection wells and supplementary wells is contained with a lower injection temperature.

Table 7. System performances at different injection water temperatures

Scenarios	Final eff. (%)	Heat loss in extracting Pro (%)	Heat loss in supplementary wells (%)
Case simulation (50°C)	71.16	2.92	12.71
Case simulation (70°C)	60.44	4.64	14.22
Case simulation 02 (90°C)	53.72	7.28	15.45

6.2.3. Practical problems and solutions

Injection/extraction discharge

In simulations, the injection discharge was constantly 4,000m^3/d, so the annual injection heat was about 1.5×10^5 MWh. However, the heat demand was not satisfied because of high thermal energy loss during the transport process. To solve this problem, the scale of ATEST system should be improved based on system efficiency.

The equation below was used to determine the needed magnification:

$$A = \frac{1}{\eta_i} \quad \ldots \quad 24$$

where η_i is the system's final efficiency of each case simulation scenario.

Results showed that, to make the requirement of heat demand, discharge in all the wells needed to be improved by 2.36 times in case simulation 01, 1.86 times in case simulation 02 and 1.58 times in case simulation 03.

Monthly well discharge

In practice, people's attention is on the heat supply instead of the extraction discharge. And the heat supply can be calculated using the equation below:

$$\text{Heat supply} = c(T_\tau - T_b)Q$$

where c is the specific heat capacity of water, T_τ is the transient temperature at the extraction well, and T_b is the background temperature. The heat supply does not totally match the extraction discharge because the temperature at the extraction well continuously decreases during extraction. As is shown in Figure 42, the peak of heat supply occurs half a month before the peak of extraction discharge.

This problem can be solved by postponing the operations of the extraction well and extracted protection wells for half a month, as is shown in Figure 42. This delay does not have obvious adverse influence because the ground surface has little impact on the ATEST system.

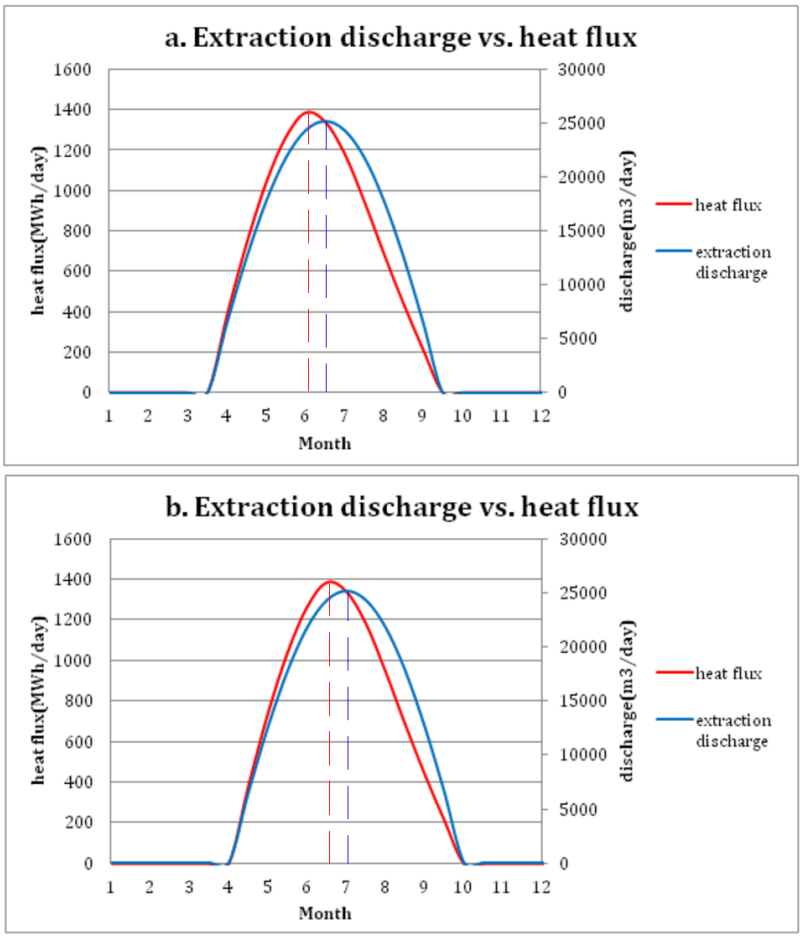

Figure 42. Monthly extraction discharge vs. monthly heat supply

6.2.4. Economic analysis

Energy aspect and COP

Since the system crosses a canal, two pump stations on both sides of the canal are needed to drive all the twelve wells, including the injection well, extraction well, protection wells and supplementary wells. Station NO.1 pumps the injection well, injected protection well and three supplementary wells, while station NO.2 pumps the extraction well, extracted protection wells, and three supplementary wells. The working principle of these two pump stations is shown in Figure 43. It can be learned that their capacities are different.

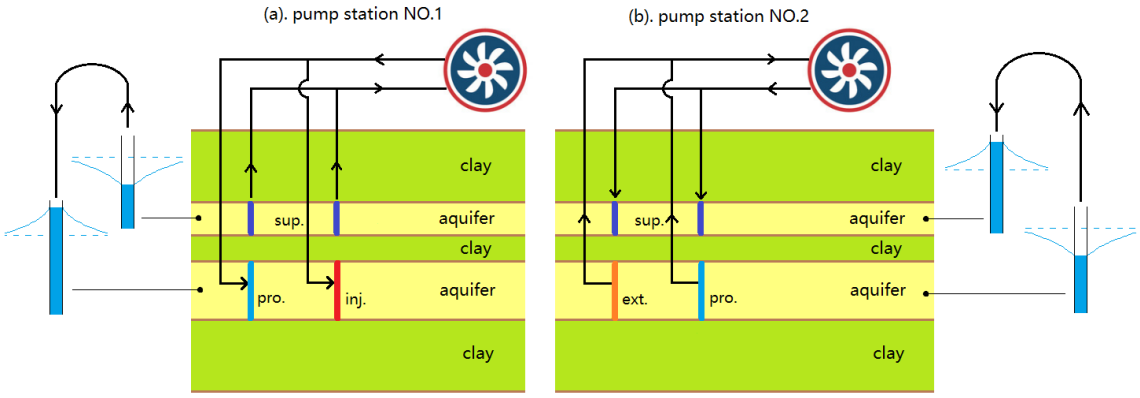

Figure 43. Working principles of pump stations

When calculating the power of the pumps, the following equation was used:

$$P = \frac{\rho g H Q}{\eta} \quad \ldots \quad 25$$

where P is the input power [KW], ρ is the water density [kg/m^3], g is the gravitational acceleration [N/kg], H is the pumped hydraulic head [m], Q is the discharge [m^3/d], and η is the efficiency of pump [-]. Each pump station drives six wells, thus:

$$HQ = \sum_1^6 (H_i Q_i) \quad \ldots \quad 26$$

$$H_i = H_s + H_f + H_l = H_s + \lambda \frac{L}{D} \frac{v^2}{2g} + \xi \frac{v^2}{2g} \quad \ldots \quad 27$$

where H_s is the static hydraulic head [m], H_f is the friction loss in pipeline [m], and H_l is local loss [m].

According to Van Beek (2011), to avoid borehole clogging, the velocity of underground flow should be lower than 1/12 of hydraulic conductivity. So the underground flow should be <0.36m/d in fine sand (K=5e-5m/s), <1.44m/d in medium sand (K=2e-4m/s), and <2.88m/d in coarse sand (K=4e-4m/s). Within this constraint, the maximum discharge for one well can be calculated using the equation below:

$$Q = vA = v(\pi d H) \quad \ldots \quad 28$$

where d is the diameter of well [m], and H is the aquifer thickness [m]. If the diameter of the well is 2m, $Q_{aquifer(1),max}$=253.3m^3/d, and $Q_{aquifer(2),max}$=208.1m^3/d. From equation 13, it is known that the driving water head can be the background water head (±0.249m) in both aquifer (1) and aquifer (2). Since the water head in aquifer (1) is about 10m above that in aquifer (2), the static hydraulic head is about 10.5m for pump station NO.1 and -9.5m for pump station NO.2.

In operation, multiple wells were needed to transport the water from/to underground, but one pipe was enough to transport water from/to the pump stations. For one pipe, to transport (4000+3000×2)×1.86m^3 water every day, the flow velocity should be 1.096m/s when the pipe diameter is 0.5m. With a 200m PVC pipe, the sum of friction loss and local loss is about 1m.

System performance was assessed using COP (coefficient of performance) as follows:

$$COP = \frac{Q}{W}$$

where Q is the useful heat supplied by ATEST system, and W is the work required by ATEST system. For case simulation Sce.02, the pump station NO.1 needs electricity of 354.6 MWh per year if the pump efficiency is 0.6, and 292.9 MWh per year for pump station NO.2. Therefore, an annual 647.5MWh is needed to transport the heat in 1.5×10^5 MWh per year, and COP=231.7.

Investment

Pump stations and pipes are two main components of both the ATES and ATEST systems. In the ATES system, one pump station is needed to drive warm water, but the transmission pipes are needed because the barriers (e.g. canal, large building) make it difficult and costly to install pipes. In the ATEST system, pipes are not needed during warm water transmission, but two pump stations are needed because the separation caused by the barriers.

According to Marzouk et al. (2011), generally, the cost of a pump station with around 8000m^3/d in capacity and 10m in hydraulic head difference is about one million Euros. And Zhao et al. (2002) estimated that the cost of 250m pipes with the laying project is about 640 thousand Euros. But for crossing a 20m barrier, the pipes should be installed by tunneling (30-50m), which is much more expensive, about 100 million Euros per kilometer (€3-5 million for 30-50m)[7]. Table 8 shows the comparison of the cost of the ATES and ATEST systems.

Table 8. Investment cost of ATEST and ATES systems

	ATEST	ATES
Pump station	2×1,000,000	1,000,000
Pipe buried		640,000
Pipe tunneled		4,000,000 (40m)
total	2,000,000	5,640,000

In conclusion, the investment cost of ATEST is much lower than that of ATES with pipes. And installing an ATEST system is much easier technologically.

[7].https://www.greaterauckland.org.nz

7. Discussion

Three ways of heat loss have been identified in this research: 1) lost to the confining layers 2) lost to the supplementary wells; 3) lost to the protection wells. In practice, it is impossible to avoid heat conduction, so the heat loss to the confining layers cannot be reduced. However, it is possible to reduce the heat loss to the supplementary wells and protection wells through: 1) reusing the warm water from the supplementary wells and reheating it to 90°C for the next heat transport, 2) lengthening the distance between the extracted protection wells and the extraction wells, and 3) installing a small well between the extraction well and extracted protection wells, as is shown in Figure 44.

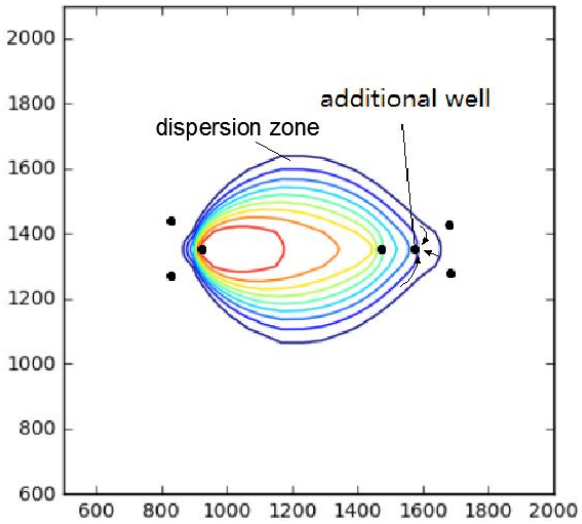

Figure 44. Warm zone with additional extraction well

In operation, the injected thermal energy should be magnitude to about 1.86 times of heat demand to compensate the heat losses during the transport process, based on the system efficiency. Considering that, in winter, the temperature of extracted water continuously decreases, the operation of extraction discharge should be postponed for about half a month to make heat supply meet the demand.

Although the impacts of different parameters and possible working conditions were identified, the ATEST systems simulated in this study have not achieved its optimal performance. In practice, a better combination of discharge in protection/injection/ extraction wells should be designed to improve the system performance.

In the case simulation, the lower aquifer was used as the main aquifer, and the upper aquifer was used for water balance. One important advantage of this layout was that less heat reached the ground surface, having a smaller influence on it. But, in practice, it is also feasible to use the upper aquifer for warm water transport and the lower aquifer for water balance, because the functions of the aquifers mainly depend on their characteristics. If both aquifers are suitable, the lower one will be the first choice. In this

research, the lower aquifer was used for warm water transport because it was thicker and had lower permeability.

It has been known from the case simulation that the system has higher recovery efficiency with a lower injection temperature. But a lower temperature means worse quality of heat, and an additional heat pump may be used to raise the temperature. In practice, an optimal temperature should be iterated that minimizes the operation cost, because heat is increasingly lost when the injection temperature is high, and the heat pump is more relied upon when it is low.

8. Conclusion

This research shows that the subsurface can be used for both heat storage and transport. An ATEST system can use an aquifer instead of pipes to transport warm water. However, it can only be used within limited distances like crossing a river or in a large building due to the heat loss during the transport process.

Additional wells are used to create a sufficiently strong hydraulic gradient to transport the heat. These so-called protection wells, however, contribute to the heat losses when located insufficiently far from the extraction well or its discharge is not adapted to the discharge of the extraction well. The thermal travel time of the ATEST system is acceptable. Besides, in the case simulation, the ATEST system can be used repeatedly.

The system performance can be affected by different parameters, and the most optimal conditions are:

- Relatively high intrinsic permeability (10^{-11}-5×10^{-11} m^2), which equals the hydraulic conductivity in 10-50m/d at 20°C, to reduce resistance in the transport process and avoid too much dispersion at the system boundary;
- Low porosity to promote groundwater flow in specific hydraulic gradient;
- Short transport distance to improve system performance in both thermal travel time and system efficiency.
- Large injection / extraction discharge and properly determined aquifer thickness to achieve the optimal operation condition;
- Large discharge in protection wells to promote transport of warm water and constrain the warm zone.

The performance of the ATEST system is acceptable when COP>200. Besides, when crossing a barrier in water transport, installing an ATEST system is much cheaper and easier than setting up an ATES system with tunneled pipes.

Reference

Bakker, M. (2015). "TimML A Multiaquifer Analytic Element Model Version 4.0 DRAFT."

Bloemendal, M. and N. Hartog (2016). AFTER THE BOOM; EVALUATION OF DUTCH ATES-SYSTEMS FOR ENERGY EFFICIENCY. European Geothermal conference.

Bloemendal, M., et al. (2014). "How to achieve optimal and sustainable use of the subsurface for Aquifer Thermal Energy Storage." Energy Policy **66**: 104-114.

Blumm, J. and A. Lindemann (2003). "Characterization of the thermophysical properties of molten polymers and liquids using the flash technique." High Temp. High Press **35**(36): 627.

Bonté, D., et al. (2012). "Subsurface temperature of the onshore Netherlands: new temperature dataset and modelling." Geologie En Mijnbouw **91**(4): 491-515.

Bonte, M., et al. (2013). Effecten en risico's van gesloten bodemenergiesystemen. Nieuwegein, KWR Watercycle research institute.

Brokx, L. (2016). "Problems encountered with and future possibilities for medium and high temperature aquifer thermal energy storage in the Netherlands. Bachelor thesis Earth Sciences." Utrecht University.

CAN GÜLEN, S. (2010). "A Proposed Definition of CHP Efficiency." Power **154**(6).

Cloetingh, S., et al. (2010). "Lithosphere tectonics and thermo-mechanical properties: An integrated modelling approach for Enhanced Geothermal Systems exploration in Europe." Earth-Science Reviews **102**(3–4): 159-206.

DiPippo, R. (2016). Geothermal Power Generation: Developments and Innovation, Woodhead Publishing.

Doughty, C., et al. (1982). "A dimensionless parameter approach to the thermal behavior of an aquifer thermal energy storage system." Water Resources Research **18**(3): 571-587.

Drijver, B. (2011). High temperature aquifer thermal energy storage (HT-ATES): water treatment in practice. Nationaal Congres Bodemenergie Proceedings.

Drijver, B., et al. (2012). High-temperature aquifer thermal energy storage (HT-ATES) - sustainable and multi-usable. Innostock 2012, the International Conference on Energy Storage.

Fitts, C. R. (2003). "Groundwater Science." Groundwater Science.

Harbaugh, A. W. (2005). MODFLOW-2005, the US Geological Survey modular ground-water model: the ground-water flow process, US Department of the Interior, US Geological Survey Reston, VA, USA.

Hart, D. J., et al. (2006). "The vertical hydraulic conductivity of an aquitard at two spatial scales." Ground Water **44**(2): 201-211.

Hubbert, M. K. (1940). "The Theory of Ground-Water Motion." Holzforschung **23**(6): 185-192.

India, M. o. P. G. o. (2015). "Normalization Document and Monitaring & Verification Guidelines-Thermal Power Plant Sector."

Ingebritsen, S. E. and W. E. Sanford (1998). Groundwater in Geologic Processes, Cambridge University Press.

Langevin, C. D., et al. (2008). SEAWAT Version 4: A computer program for simulation of multi-species solute and heat transport, Geological Survey (US).

Lee, C. K. and S. P. Yim (2007). "Hydrodynamic dispersion coefficients in a porous medium with parallel fractures."

Marzouk, M. M. and R. M. Ahmed (2011). "A case-based reasoning approach for estimating the costs of pump station projects." Journal of Advanced Research **2**(4): 289-295.

Niessink, R. and H. Rösler (2015). Development of Heat Distribution Networks in the Netherlands, Petten: ECN.

Nishigaki, H. (2005). "Trends and Future Outlook for Thermal Power Plants."

Nordell, B., et al. (2015). 5–The use of aquifers as thermal energy storage (TES) systems.

Novo, A. V., et al. (2010). "Review of seasonal heat storage in large basins: Water tanks and gravel–water pits." Applied Energy **87**(2): 390-397.

Paksoy, H., et al. (2009). "State-of-the-Art Review of Aquifer Thermal Energy Storage Systems for Heating and Cooling Buildings."

Paksoy, H. Ö. (2007). Thermal energy storage for sustainable energy consumption: fundamentals, case studies and design, Springer Science & Business Media.

Parlange, J. Y. (1973). "Dynamics of Fluids in Porous Media by J. BEAR." American Scientist(6): 758-759.

Plc, B. P. (2016). "BP Energy Outlook 2016."

Pluymaekers, M., et al. (2012). "Reservoir characterisation of aquifers for direct heat production: Methodology and screening of the potential reservoirs for the Netherlands." Netherlands Journal of Geosciences **91**(04): 621-636.

Price, W. G., et al. (1911). "Discussion of Dams on Sand Foundations: Some Principles Involved in Their Design, and the Law Governing the Depth of Penetration Required for Sheet-Piling by Arnold C. Koenig." Transactions of the American Society of Civil Engineers.

Rathakrishnan, E. (2005). Fundamentals of engineering thermodynamics, PHI Learning Pvt. Ltd.

Sanner, B., et al. (2005). "Underground Thermal Energy Storage for the German Parliament in Berlin, system concept and operational experiences." 24-29.

Sanner, B., et al. (2003). "Current status of ground source heat pumps and underground thermal energy storage in Europe." Geothermics **32**(4): 579-588.

Sommer, W., et al. (2015). "Optimization and spatial pattern of large-scale aquifer thermal energy storage." Applied Energy **137**: 322-337.

Streeter and VictorL (1979). Fluid mechanics. /-7th ed, McGraw-Hill.

Theis, C. V. (1935). "The relation between the lowering of the Piezometric surface and the rate and duration of discharge of a well using ground‐water storage." Eos Transactions American Geophysical Union **16, pt. 2**(2): 519-524.

Thorne, D., et al. (2006). "Addition of simultaneous heat and solute transport and variable fluid viscosity to SEAWAT." Computers & Geosciences **32**(10): 1758-1768.

Timms, W., et al. (2014). "Vertical hydraulic conductivity of a clayey-silt aquitard: accelerated fluid flow in a centrifuge permeameter compared with in situ conditions." Hydrology and Earth System Sciences Discussions **11**(3): 3155-3212.

Toth, A. and E. Bobok (2016). Flow and Heat Transfer in Geothermal Systems.

Tsang, C. F. (2012). "Aquifer thermal energy storage-a survey."

van Beek, C. K. (2011). Cause and prevention of clogging of wells abstracting

groundwater from unconsolidated aquifers, IWA Publishing.

van Lopik, J. H., et al. (2016). "The use of salinity contrast for density difference compensation to improve the thermal recovery efficiency in high-temperature aquifer thermal energy storage systems." Hydrogeology Journal **24**(5): 1255-1271.

van Lopik, J. H., et al. (2015). "Salinization in a stratified aquifer induced by heat transfer from well casings." Advances in water resources **86**: 32-45.

Verkaik, J., et al. (2011). "MT3DMS, A Modular Three-Dimensional Multispecies Transport Model."

Voss, C. I. (1984). "A finite-element simulation model for saturated-unsaturated, fluid-density-dependent ground-water flow with energy transport or chemically-reactive single-species solute transport."

Wesselink, M. (2016). "Prospects for HT-ATES in the Dutch energy system."

Willemsen, N. (2016). "Rapportage bodemenergiesystemen in Nederland." RVO/IF technology, Arnhem.

Zangheri, P., et al. (2014). "Heating and cooling energy demand and loads for building types in different countries of the EU." Polytechnic University of Turin, end-use Efficiency Research Group.

Zeghici, R. M., et al. (2015). "Integrated assessment of variable density–viscosity groundwater flow for a high temperature mono-well aquifer thermal energy storage (HT-ATES) system in a geothermal reservoir." Geothermics **55**: 58-68.

Zhao, J. and B. Rajani (2002). "Construction and rehabilitation costs for buried pipe with a focus on trenchless technologies. National Research Council." Institute for research in construction, Ottawa, Canada.

Acknowledgement

I achieved this research by the help from Prof. Mark Bakker, Ir. Martin Bloemendal, Dr. Niels Hartog and Dr. Boris van Breukelen.

Thanks to the advising from Mr. Martin that I could keep the right way in this research, his suggestions helped me to find proper solutions when I met problems, and his positive attitude kept me motivated throughout the entire process. Thanks to the guidance from Mr. Mark that I could found and solve the problems in my research, I do have dramatic improvement in my study after following his ideas. Thanks to the ideas from Mr. Neils that I could achieve this creative research. I also want to thank Mr. Boris, by his suggestion I could finish a paper with higher quality.

Thanks to my parents, without them I was not able to have the study chance in the Netherlands, and then be more capable to have a promising future. I want to thank all my classmates in Water Management, by their help and the group work with them I could achieve many challengeable courses in these two years. I also want to thank my friends in the Netherlands; with them I could solve the problems in my daily life and have a happy life here.